

IGF-1 Receptor Differentially Regulates Spontaneous and Evoked Transmission via Mitochondria at Hippocampal Synapses

Highlights

- Presynaptic IGF-1Rs are basally active in hippocampal neurons
- IGF-1R tone enhances evoked transmission, while inhibiting spontaneous transmission
- Mitochondrion is a differential regulator of synaptic transmission by IGF-1Rs
- IGF-1R tone buffers resting Ca^{2+} and maintains ATP levels during spiking activity

Authors

Neta Gazit, Irena Vertkin, Ilana Shapira, ..., Yael Mor, Silvio Rizzoli, Inna Slutsky

Correspondence

islutsky@post.tau.ac.il

In Brief

Gazit et al. demonstrate that presynaptic IGF-1R tone enhances evoked while suppressing spontaneous synaptic vesicle release in hippocampal neurons. Mitochondria, activated by IGF-1Rs, constitute a differential regulator of information processing by maintaining evoked-to-spontaneous transmission ratio, while constraining synaptic high-pass filtering.

IGF-1 Receptor Differentially Regulates Spontaneous and Evoked Transmission via Mitochondria at Hippocampal Synapses

Neta Gazit,^{1,2} Irena Vertkin,¹ Ilana Shapira,¹ Martin Helm,^{3,4} Edden Slomowitz,¹ Maayan Sheiba,¹ Yael Mor,^{1,2} Silvio Rizzoli,³ and Inna Slutsky^{1,2,*}

¹Department of Physiology and Pharmacology, Sackler Faculty of Medicine, Tel Aviv University, 69978 Tel Aviv, Israel

²Sagol School of Neuroscience, Tel Aviv University, 69978 Tel Aviv, Israel

³Department of Neuro- and Sensory Physiology, Cluster of Excellence Nanoscale Microscopy and Molecular Physiology of the Brain, European Neuroscience Institute, University of Göttingen Medical Center, 37075 Göttingen, Germany

⁴International Max Planck Research School Molecular Biology, 37077 Göttingen, Germany

*Correspondence: islutsky@post.tau.ac.il

<http://dx.doi.org/10.1016/j.neuron.2015.12.034>

This is an open access article under the CC BY-NC-ND license (<http://creativecommons.org/licenses/by-nc-nd/4.0/>).

SUMMARY

The insulin-like growth factor-1 receptor (IGF-1R) signaling is a key regulator of lifespan, growth, and development. While reduced IGF-1R signaling delays aging and Alzheimer's disease progression, whether and how it regulates information processing at central synapses remains elusive. Here, we show that presynaptic IGF-1Rs are basally active, regulating synaptic vesicle release and short-term plasticity in excitatory hippocampal neurons. Acute IGF-1R blockade or transient knockdown suppresses spike-evoked synaptic transmission and presynaptic cytosolic Ca^{2+} transients, while promoting spontaneous transmission and resting Ca^{2+} level. This dual effect on transmitter release is mediated by mitochondria that attenuate Ca^{2+} buffering in the absence of spikes and decrease ATP production during spiking activity. We conclude that the mitochondria, activated by IGF-1R signaling, constitute a critical regulator of information processing in hippocampal neurons by maintaining evoked-to-spontaneous transmission ratio, while constraining synaptic facilitation at high frequencies. Excessive IGF-1R tone may contribute to hippocampal hyperactivity associated with Alzheimer's disease.

INTRODUCTION

IGF-1R signaling pathway is genetically preserved throughout evolution and is essential for normal development, growth, and survival (D'Ercole et al., 1996). Reduction in the IGF-1R signaling represents a highly conserved mechanism of lifespan extension and delays aging in diverse species, including yeast, worms, fruit flies, and rodents (Kenyon, 2010). Moreover, mutations leading to partial loss of function in the IGF-1R are associated with

exceptional longevity in humans (Suh et al., 2008). As aging is the major risk factor for the development of Alzheimer's disease (AD) and other neurodegenerative disorders (Amaducci and Tesco, 1994), it is plausible that reduction in the IGF-1R signaling may augment ability of neural circuits to delay the onset of neurodegeneration (Cohen and Dillin, 2008). Genetic reduction in the IGF-1R level has been shown to rescue AD-like pathology, synaptic, and cognitive deficits (Cohen et al., 2009; Freude et al., 2009; Gontier et al., 2015). On the other hand, IGF-1 was suggested as a potent neuroprotective hormone by other studies (Carro et al., 2002, 2006). These conflicting results underscore a gap in our understanding of the basic relationships between IGF-1R activity and neuronal functions.

The IGF-1R belongs to a family of transmembrane receptor tyrosine kinases (RTKs), which includes the highly homologous insulin receptor (IR) and IR-related receptors (LeRoith et al., 1995; Ullrich et al., 1986). The IGF-1R forms constitutive homodimers that undergo ligand-dependent conformational change upon activation (Lemmon and Schlessinger, 2010). IGF-1R displays high (0.16 nM) binding affinity toward IGF-1, while 100 lower affinity for insulin (Adams et al., 2000; Schumacher et al., 1991). IGF-1Rs are widely expressed in the brain, specifically in the hippocampus, olfactory bulb, cortex, choroid plexus, and cerebellum (Kar et al., 1993).

Evidence that IGF-1R and IGF-1 are involved in processes at long timescales is substantial. IGF-1 or IGF-1R deletions profoundly reduce brain size, while IGF-1R overexpression results in brain overgrowth (D'Ercole et al., 1996; Fernandez and Torres-Alemán, 2012). Blockade of synaptotagmin10-mediated IGF-1 secretion reduces neuronal size and synapse number in olfactory bulb (Cao et al., 2011). Moreover, IGF-1R blockade prevents exercise-induced neurogenesis in the hippocampus (Ding et al., 2006). Injection of IGF-1 prevents effects of monocular deprivation on ocular dominance plasticity in the visual cortex (Tropea et al., 2006) and mediates the effect of enriched environment on retinal development (Landi et al., 2009) and hippocampal neurogenesis (Trejo et al., 2001).

Despite substantial progress in understanding the role of IGF-1R signaling at extended timescales, whether IGF-1R is directly

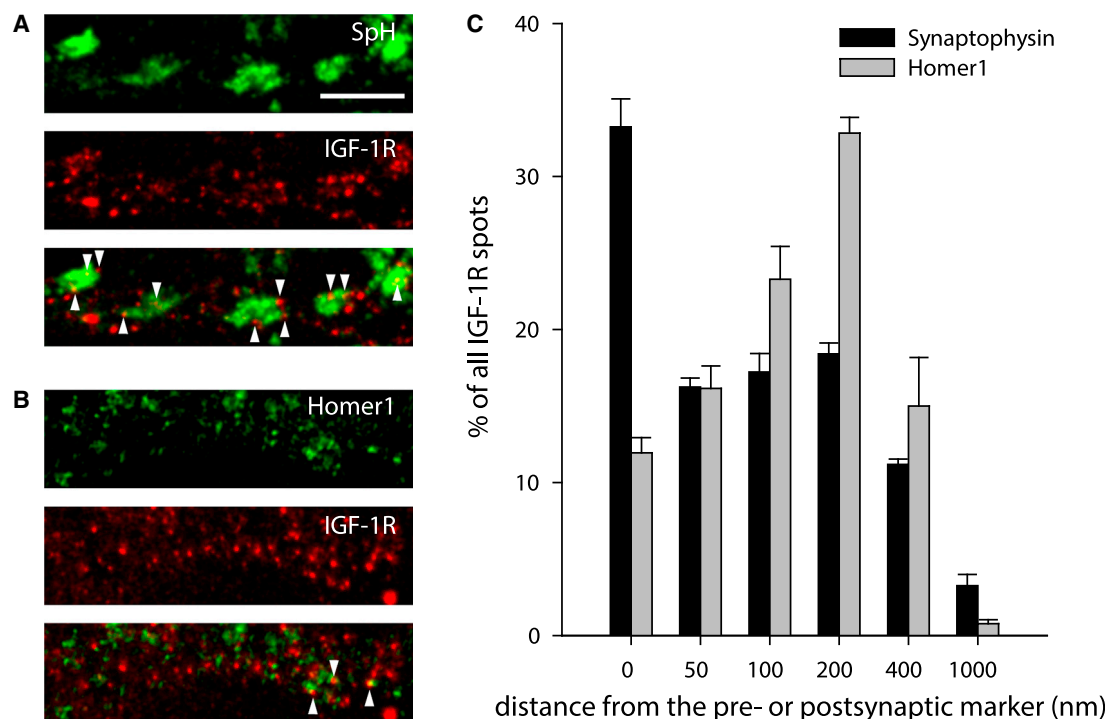


Figure 1. Synaptic Localization of IGF-1R

(A and B) Hippocampal neurons stained for IGF-1R and synaptophysin (A, presynaptic marker) or Homer1 (B, postsynaptic marker) and imaged in dual-color STED microscopy. The receptor is often found within, or close to, presynaptic terminals and also occasionally near postsynaptic structures (the arrowheads point to a few examples). The scale bar represents 2 μ m.

(C) A quantification of the distances from IGF-1Rs to the pre or postsynaptic structures. Overall, ~75% of all receptors are found within the pre or postsynaptic compartments (distances 0–50 nm from the markers). The bars show means \pm SEM from three independent experiments with ~500–3,000 receptor spots analyzed in each experiment.

involved in the regulation of information processing in central neural circuits on short timescales remains largely unknown. Only a handful of studies, utilizing supra-physiological concentrations of IGF-1, addressed this question and obtained heterogeneous results. Acute application of IGF-1 or its analog des-IGF-1 have been reported to potentiate excitatory synaptic transmission through either presynaptic (Xing et al., 2007) or postsynaptic (Ramsey et al., 2005) mechanisms, to modulate voltage-gated calcium channels (VGCCs) (Blair and Marshall, 1997), and to increase intrinsic neuronal excitability (Wang et al., 2014). The lack of information on the role of IGF-1Rs in synaptic transfer is particularly striking in comparison to the extensive research on functions of other RTKs, such as the Trk receptor family for neurotrophic factors, in synaptic transmission and plasticity (Poo, 2001). Therefore, understanding whether and how IGF-1Rs directly regulate synaptic transfer of physiologically relevant spiking patterns is important.

To address this question, we examined the relationship between IGF-1R activity/expression level, synaptic vesicle release, synaptic transmission, and short-term plasticity in primary hippocampal cultures and in acute hippocampal slices. Utilizing super-resolution imaging and fluorescence resonance energy transfer (FRET) methodology, we found that presynaptic IGF-1Rs are normally activated under resting conditions, maintaining evoked release probability (P_r), while suppressing spontaneous

vesicle release at hippocampal synapses. Our study identified mitochondrion as a differential regulator of evoked and spontaneous synaptic vesicle exocytosis by IGF-1R tone.

RESULTS

Basal IGF-1 Activates IGF-1R Signaling Pathway in Hippocampal Boutons

To assess the role of IGF1-R activity in normal neuronal function, we first asked where IGF1-Rs are expressed in hippocampal neurons. We used dual-color stimulated emission depletion (STED) microscopy, a diffraction-unlimited technique, to investigate IGF-1R localization with a resolution of ~50 nm (Revelo et al., 2014). We found that IGF-1Rs are mostly present at, or in the vicinity of, presynaptic terminals marked by synaptophysin, and to a lesser extent near postsynaptic structures marked by Homer1 (Figures 1A and 1B). In total, ~75% of all IGF-1Rs were found at synapses (at a distance of \leq 50 nm from pre or postsynaptic markers; Figure 1C), whereas ~74% of synaptic IGF-1Rs were localized at the presynaptic site.

To examine whether presynaptic IGF1-Rs are basally activated in hippocampal synapses under spontaneous synaptic activity, we developed a method to estimate IGF-1R activation at the single-synapse level in live neurons. Given that IGF-1R homodimers are activated by ligand-induced conformational

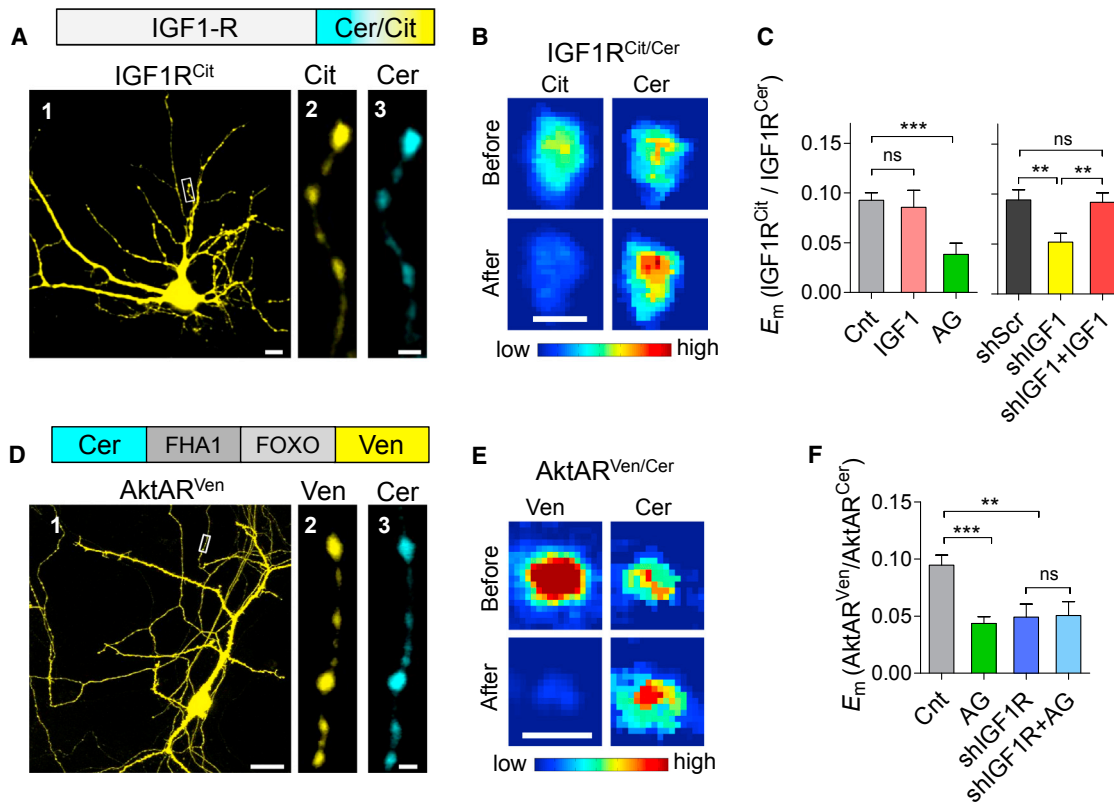


Figure 2. IGF-1R Activity Is Saturated by Basal IGF-1 in the Vicinity of Hippocampal Synapses

(A) An illustration of the IGF-1R construct tagged with Citrine (Cit) or Cerulean (Cer) (top). The representative confocal images of a hippocampal neuron expressing IGF1R^{Cit/Cer} are shown (bottom). The white box in (A₁) corresponds to the blow-ups in (A₂) and (A₃). The scale bars represent: A₁, 20 μ m and A_{2,3}, 2 μ m. (B) Pseudocolor-coded fluorescence images of IGF1R^{Cit/Cer} before and after Cit photobleaching. The scale bar represents 1 μ m. (C) IGF1R^{Cit}/IGF1R^{Cer} shows basal levels of E_{TTX} ($n = 173$ boutons) (left). The E_m was reduced by AG1024 (1 μ M, 20 min, $n = 56$), while unaffected by the addition of 50 ng/ml hIGF-1 ($n = 36$). The infection with shIGF1 ($n = 79$) reduced the E_m , compared with the shScr sequence infection ($n = 62$), the addition of hIGF1 rescued the shIGF1-induced E_m reduction ($n = 77$) (right). (D) The AktAR FRET reporter of Akt activity (Gao and Zhang, 2008) tagged with Venus (Ven) and Cerulean (Cer) (top). The representative confocal images of a hippocampal neuron expressing AktAR are shown (bottom). The white box in (D₁) corresponds to the blow-ups in (D₂) and (D₃). The scale bars represent: D₁, 20 μ m and D_{2,3}, 2 μ m. (E) Pseudocolor-coded fluorescence images of a bouton expressing AktAR, displaying donor dequenching after acceptor photobleaching. The scale bar represents 1 μ m. (F) AktAR FRET in hippocampal boutons was significantly reduced from Cnt ($n = 114$) by 1 μ M AG1024 ($n = 124$) and by IGF1R KD ($n = 46$). The AG1024 was ineffective on AktAR FRET in IGF1-KD neurons ($n = 32$). (* $p < 0.05$, ** $p < 0.01$, and *** $p < 0.001$) (ANOVA analysis with post hoc Bonferroni's multiple comparison tests). The error bars represent SEM.

changes (Lemmon and Schlessinger, 2010), we measured FRET between IGF-1R homodimers (Kavran et al., 2014). We transfected hippocampal cultures with IGF-1R C-terminally tagged with mCitrine (IGF-1R^{Cit}) and with Cerulean (IGF-1R^{Cer}) and performed FRET measurements at hippocampal boutons (Figure 2A). To estimate IGF-1R homomeric interactions, we measured the steady-state mean FRET efficiency (E_m) utilizing the acceptor photobleaching method, which dequenches the donor (Cer). E_m was measured in the presence of tetrodotoxin (TTX) which blocks spike generation, allowing only miniature synaptic release. High-magnification confocal images show an increase in Cer fluorescence after Cit photobleaching (Figure 2B), indicating dequenching of the donor and the presence of FRET. On average, IGF-1R^{Cer}/IGF-1R^{Cit} E_m was 0.092 ± 0.007 across hippocampal boutons (Figure 2C, left). To examine whether

endogenously released IGF-1 activates IGF-1Rs in the vicinity of synapses, we measured the effect of an IGF-1R inhibitor tyrostatin AG1024. AG1024 prevents binding of the substrate and ATP at the receptor phosphorylation site and binds IGF-1R with higher affinity comparing to IR (Párrizas et al., 1997). AG1024 (1 μ M) reduced E_m by 60% to 0.038 ± 0.01 , indicating that IGF-1Rs are activated under basal conditions in hippocampal neurons. Surprisingly, addition of recombinant human IGF-1 (hIGF-1, 50 ng/ml) did not affect E_m , indicating that IGF-1Rs are saturated under basal conditions. To verify whether endogenously released IGF-1 activates IGF-1Rs, we used lentiviral-based short hairpin (shRNA) methodology to knock down (KD) endogenous IGF-1. While the control hairpin (shScr) had no impact on E_m , silencing of IGF-1 by the effective hairpin shIGF-1 (~50% KD; Figures S1A and S1B) resulted in a

45% reduction of E_m (Figure 2C, right). Moreover, E_m was completely rescued by application of hIGF-1 in neurons infected with shIGF-1 (Figure 2C, right). E_m did not correlate to the donor-to-acceptor ratio in our experiments (Figure S2A), excluding it as a potential source of variability.

Next, we asked whether endogenously active IGF-1Rs stimulate Akt, a canonical substrate downstream of the IGF-1R. For this purpose, we used the FRET reporter of Akt activity (AktAR; Figure 2D) that contains Cer at the N terminus of the FHA1 domain and Venus (Ven) variant cpVE172 at the C terminus of the substrate region (Gao and Zhang, 2008). AG1024 decreased E_m by 54% from 0.093 ± 0.009 to 0.043 ± 0.006 (Figures 2E and 2F), suggesting that IGF-1R significantly contributes to basal Akt activity at synapses. FRET measurements did not depend on the donor-to-acceptor ratio (Figure S2B). Similar results were obtained by FRET ratio method, enabling FRET comparison per synapse (Figure S2C).

To verify whether AG1024 reduces Akt activity selectively via the IGF-1R, we used shIGF-1R to KD endogenous IGF-1Rs. We selected a sequence that causes efficient IGF-1R KD in hippocampal neurons (Figure S1). AktAR FRET was reduced to 0.045 ± 0.01 by shIGF-1R (Figure 2F), similarly to the level produced by AG1024 inhibitor. Moreover, AktAR FRET lost its sensitivity to AG1024 in shIGF-1R infected neurons (Figure 2F), indicating the specificity of AG1024 effect. Altogether, these results strongly suggest that IGF-1R signaling is activated under basal conditions in hippocampal neurons.

IGF-1R Blockade or KD Attenuates Evoked Synaptic Vesicle Release

Next, we explored whether endogenously released IGF-1 modulates basal synaptic Pr . We estimated the effect of pharmacological blockade of IGF-1Rs and its KD on presynaptic strength using activity-dependent FM dye (Abramov et al., 2009). First, we measured the density (D) and the intensity (ΔF) of activity-dependent FM1-43 dye uptake to presynaptic vesicles turned over by stimulation of 30 action potentials (APs) at a rate of 0.5–1 Hz in cultured hippocampal neurons (Figure S3A). We quantified the total presynaptic strength ($S = \Delta F \times D$) before and 15 min after addition of 1 μ M AG1024. Inhibition of IGF-1Rs by AG1024 induced a substantial decrease in both ΔF and D across synaptic populations, resulting in 53% reduction in the total S in hippocampal neurons (Figures 3A–3C). To determine the effect of AG1024 on vesicle exocytosis per se, we measured the rate of FM1-43 destaining during low-frequency stimulation. The experimental protocol described above was modified for staining of the total pool of recycling vesicles by 600 APs at 20 Hz and destaining by 1 Hz stimulation (Figure S3B). AG1024 decreased the destaining rate constant ($k = 1/\tau_{\text{decay}}$, where τ_{decay} is an exponential time course) by 34% (Figure 3D), suggesting inhibition of the exocytosis rate. As a result of the IGF-1R-mediated presynaptic inhibition, mean firing rate of spontaneous spikes was reduced (Figure S4).

Due to a high homology between the IGF-1R and the IR, we examined the effects of two additional IGF-1R inhibitors displaying different mechanisms of action: (1) α IR3, a neutralizing antibody raised against the IGF-1R, preventing IGF-1 binding and

blocking IGF-1-mediated receptor activation (Flier et al., 1986); and (2) picropodophyllin (PPP), a small toxin molecule, penetrating the cell membrane and inhibiting the receptor at the intracellular, substrate binding domain. PPP has been shown to specifically inhibit IGF-1R, but not IR (Vasilcanu et al., 2004). As both inhibitors require a longer time period to block IGF-1R activity, we pretreated the neuronal cultures for 3–4 hr with either PPP (1 μ M) or α IR3 (1 μ g/ml) before testing their effect on presynaptic function. The total S was reduced by 37% following PPP and by 29% following α IR3 treatments (Figure 3E).

Next, we asked whether the effect of pharmacological IGF-1R blockade on Pr can be mimicked by transient downregulation of IGF-1R expression in hippocampal neurons. Indeed, shIGF-1R reduced the total S by 50% (Figure 3F) without affecting the total vesicle recycling pool (Figure S5A). Importantly, the IGF-1R KD phenotype was rescued by shRNA-resistant wild-type IGF-1R (Figures 3F, S1D, and S1E). The effect of AG1024 on Pr was occluded by IGF-1R KD (Figures 3F and S5B), confirming the specificity of AG1024 effect.

Finally, we assessed the effect of ectopically applied IGF-1 on synaptic vesicle release. Acute application of recombinant IGF-1 from different sources (human or rat IGF-1 or des-(1-3) IGF-1 analog) did not alter basal synaptic vesicle recycling (Figure 3G), confirming saturation of presynaptic IGF-1Rs by extracellular IGF-1 as suggested by the FRET-based assessment of IGF-1R activation (Figures 2A–2C). Importantly, IGF-1 KD inhibited synaptic vesicle exocytosis and this effect was rescued by IGF-1 application (Figure 3H). Based on these results, we conclude that extracellular, local IGF-1 in the vicinity of synapses is important for maintenance of synaptic vesicle release evoked by low-frequency spikes in hippocampal neurons (Figure 3I).

IGF-1R Blockade Inhibits Basal CA3-CA1 Synaptic Transmission

Having established an essential role of IGF-1R basal activity in regulating synaptic vesicle release in hippocampal cultures, we asked whether acute IGF-1R inhibition modulates basal synaptic transmission in a more intact preparation, acute hippocampal slices. We evoked electrical stimulation in CA3 axons, comprising the Schaffer Collateral (SC) pathway of the hippocampus, and recorded the extracellular field excitatory postsynaptic potentials (fEPSP) in the stratum radiatum or EPSCs using whole-cell patch-clamp technique (Figure 4A). We estimated the effect of AG1024 (1 μ M, 30 min) on basal CA3-CA1 synaptic transmission evoked by low-frequency stimulation of 0.1 Hz. AG1024 caused a gradual reduction in the fEPSP amplitude (Figure 4B), resulting in a 47% decrease of the slope of input/output curve (Figure 4C). Moreover, AG1024 caused a robust and pronounced 73% inhibition of the AMPA receptor (AMPA)-mediated EPSC amplitude, measured at -70 mV (Figure 4D). Contrary to an earlier study in rat hippocampal slices (Ramsey et al., 2005), we did not observe any effect of des-(1-3)IGF-1 (50 ng/ml, 30 min) on CA3-CA1 synaptic transmission in mouse hippocampal slices (Figure S6). Thus, our data indicate that IGF-1Rs are basally active under low-frequency stimulation, contributing to synaptic transmission in CA3-CA1 hippocampal connections.

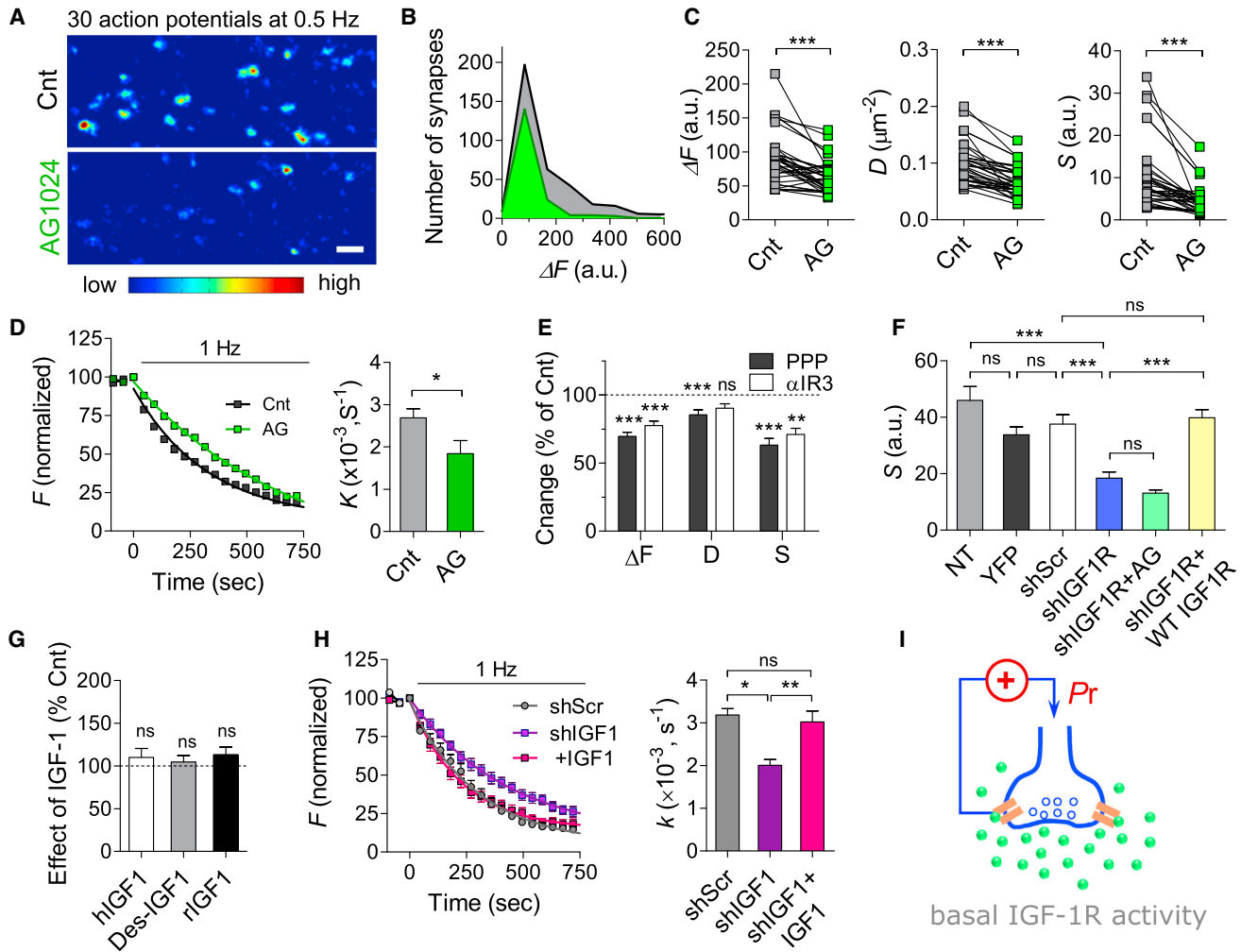


Figure 3. Pharmacological Blockade and KD of IGF-1R Induces a Decrease in Pr via Inhibition of Presynaptic Ca^{2+} Flux

(A) Representative high-magnification ΔF images before and 15 min after application of 1 μM AG1024. The stimulation protocol during FM dye staining: 30 APs at 1 Hz. The scale bar represents 2 μm . The fluorescence intensities (arbitrary units, a.u.) are coded using pseudocolor.

(B) ΔF histograms before (Cnt) and after AG1024 application (AG) in a single experiment. The median ΔF decreased from 99 to 51 a.u. and the number of FM-(+) puncta decreased from 582 to 239.

(C) Acute application of AG1024 reduced ΔF , D , and S across synaptic populations in 11 experiments.

(D) Representative traces (left) and summary of AG1024 effect (right) on the destaining rate constant (k) during 1 Hz stimulation at hippocampal boutons. AG1024 decreased averaged k from $(2.7 \pm 0.02) \times 10^{-3}$ to $(1.8 \pm 0.03) \times 10^{-3} s^{-1}$ ($n = 6$ for each condition).

(E) Inhibition of IGF-1R by PPP (3 hr, 1 μM , and $n = 46$) or $\alpha IR3$ (4 hr, 1 $\mu g/ml$, and $n = 42$) decreased ΔF , D , and S .

(F) Summary of shIGF-1R effect on presynaptic vesicle recycling ($n = 24$) compared to non-infected ($n = 21$), YFP only ($n = 15$) and shScr ($n = 26$) infected neurons. The shIGF1R induced a 2-fold reduction in S compared to shScr. The AG1024 did not further reduce S ($n = 11$). Infection with the WT IGF1R rescues the effect of IGF-1R KD ($n = 19$).

(G) Effect of IGF-1 (50 ng/ml, 20 min) on presynaptic vesicle recycling (normalized to Cnt). There was no significant effect ($p > 0.1$) of human IGF-1 (hIGF1, $n = 31$), rat IGF-1 (rIGF1, $n = 4$), or Des-(1-3)IGF-1 analog (Des-IGF1, $n = 16$) as shown.

(H) Representative traces of the destaining rate constant (k) during 1 Hz stimulation in cultures infected by shScr ($n = 4$) and shIGF-1 ($n = 5$). The hIGF-1 ($n = 6$, 50 ng/ml, and 20 min preincubation) rescued vesicle exocytosis in shIGF-1 neurons.

(I) Illustration of the positive Pr regulation by basal IGF-1R activity in Pr regulation (* $p < 0.05$, ** $p < 0.01$, and *** $p < 0.001$). The error bars represent SEM.

IGF-1R Regulates Short-Term Synaptic Plasticity under Physiological and Pathological Conditions

Having established a causal relationship between IGF-1R activity and basal synaptic vesicle release, we examined how inhibition of IGF-1R activation affects vesicle release and synaptic transmission evoked by high-frequency spike bursts. Given the inverse

relationship between Pr and synaptic facilitation (Dobrunz and Stevens, 1997), we expected an increase in short-term facilitation by IGF-1R blockade. To test this prediction, we examined the effect of AG1024 on short-term plasticity (STP) in hippocampal slices by measuring EPSCs, recorded at -70 mV, during high-frequency spike bursts in CA3-CA1 synaptic connections in acute

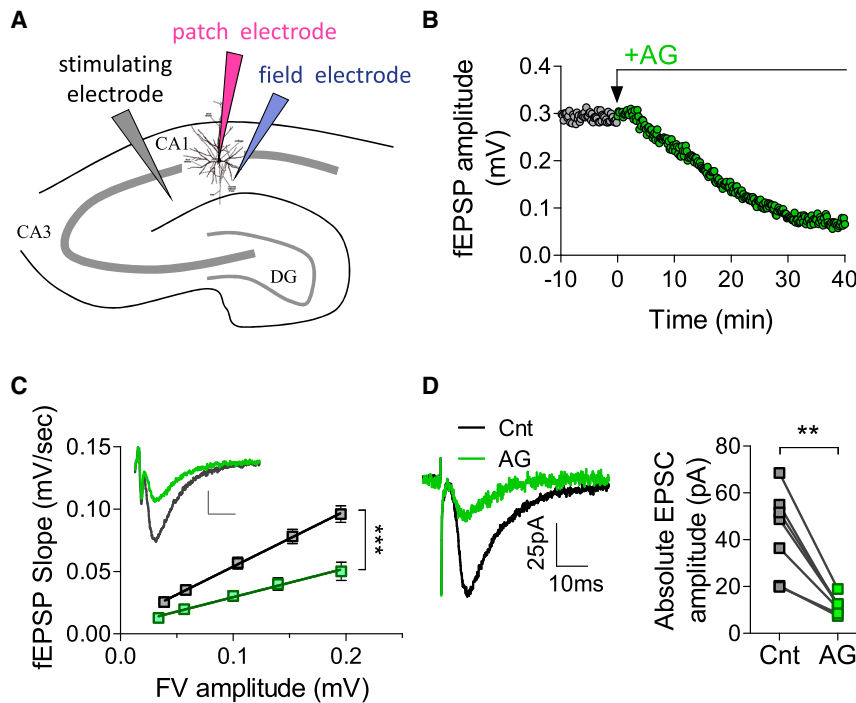


Figure 4. IGF-1R Blockade Induces a Reduction in AMPAR-Mediated EPSC in CA3-CA1 Hippocampal Connections

(A) Experimental setup and CA3-CA1 organization. (B) Time course of AG1024 effect on fEPSP amplitude. (C) Representative fEPSP recordings before (gray) and 60 min after (green) application of AG1024 under low-frequency stimulation (0.1 Hz) (top). The scale bars represent 0.1 mV and 10 ms. The AG1024 reduced the input-output relationship between the intensity of the fiber volley amplitude and the fEPSP slope ($n = 19$) (bottom). (D) Representative EPSC recordings (holding potential -70 mV) before (gray) and 60 min after (green) application of AG1024 under low-frequency stimulation (0.1 Hz) (left). The summary of the effect of AG1024 on EPSC amplitude (student paired two-tailed t test and $n = 7$) (right) (** $p < 0.01$ and *** $p < 0.001$). The error bars represent SEM.

Increased IGF-1R expression was observed in human AD brains (Moloney et al., 2010) and in the APP/PS1 transgenic AD mouse model (Zhang et al., 2013). Therefore, we hypothesized that augmented IGF-1R expression may contribute to increased basal synaptic transmission and reduced STP, which can represent very early synaptic dysfunctions in APP/PS1 mice (Dolev et al., 2013). Mice were examined at the early stage (6–8 weeks), before the appearance of amyloid plaques (Jankowsky et al., 2004). Basal CA3-CA1 synaptic transmission was significantly higher in slices of APP/PS1 mice (Figure 5G), resulting in an increase in the input/output (I/O) relationship (Figure 5H). The short-term facilitation in CA3-CA1 connections of APP/PS1 mice was significantly lower than in wild-type mice (Figures 5G and 5I), indicating higher *Pr*. Blockade of basal IGF-1R activity by AG1024 led to a pronounced reduction in basal synaptic transmission (Figures 5G and 5H) with concomitant increase in short-term facilitation (Figures 5G and 5I) in APP/PS1 hippocampal connections. Surprisingly, the I/O relationship and synaptic facilitation were indistinguishable between wild-type (WT) and APP/PS1 connections following IGF-1R blockade. Notably, blockade of other RTK receptors, such as Trks, by K252a inhibitor did not affect synaptic transmission and STP in either WT or APP/PS1 model (Figure S7). These results indicate that enhanced IGF-1R-mediated augmentation of excitatory synaptic transmission may contribute to AD-related hippocampal hyperactivity.

hippocampal slices. Application of AG1024 resulted in a decrease of the first EPSC amplitude within the burst, but its effect on the last amplitude was less pronounced (Figure 5A). On average ($n = 7$), AG1024 profoundly increased short-term synaptic facilitation as estimated by increase in the relative EPSC amplitude within the burst (Figure 5B). Moreover, STP was increased by other types of IGF-1R inhibitors, namely PPP and α IR3 antibody in hippocampal cultures (Figures S3C–S3E). Taken together, these results suggest that basal IGF-1R activity fine-tunes the filter properties of hippocampal synaptic connections by maintaining an appropriate level of facilitation.

Next, we asked how STP is affected by changes in the level of IGF-1R expression. For this purpose, we altered IGF-1R expression in hippocampal cultures using shRNA KD strategy versus overexpression of IGF-1R fused to cyan fluorescent protein (CFP). The magnitude and the sign of short-term presynaptic plasticity (S_{burst} / S_{single}) was calculated by dividing the total number of vesicles recycled due to bursts by the number of vesicles recycled by a similar number of single spikes in the same population of synapses (Abramov et al., 2009). $S_{burst} / S_{single} > 1$ reflects short-term facilitation. IGF-1R KD resulted in a 55% decrease of S_{single} (Figures 5C and 5D), without affecting S_{burst} (Figures 5C and 5E). As a result, short-term synaptic facilitation was increased by 61% (Figure 5F) and rescued by knock in of shRNA-resistant IGF-1R (Figure S3F). Conversely, overexpression of IGF-1R (OE) completely abolished synaptic facilitation (Figure 5F) due to 4.4-fold increase in S_{single} (Figures 5C and 5D) and only 1.6-fold increase in S_{burst} (Figures 5C and 5E). Thus, regulation of IGF-1R expression bi-directionally modulates short-term facilitation in hippocampal synapses. Moreover, optimal level of IGF-1R activation is needed to keep short-term synaptic plasticity in a physiological range.

contribute to increased basal synaptic transmission and reduced STP, which can represent very early synaptic dysfunctions in APP/PS1 mice (Dolev et al., 2013). Mice were examined at the early stage (6–8 weeks), before the appearance of amyloid plaques (Jankowsky et al., 2004). Basal CA3-CA1 synaptic transmission was significantly higher in slices of APP/PS1 mice (Figure 5G), resulting in an increase in the input/output (I/O) relationship (Figure 5H). The short-term facilitation in CA3-CA1 connections of APP/PS1 mice was significantly lower than in wild-type mice (Figures 5G and 5I), indicating higher *Pr*. Blockade of basal IGF-1R activity by AG1024 led to a pronounced reduction in basal synaptic transmission (Figures 5G and 5H) with concomitant increase in short-term facilitation (Figures 5G and 5I) in APP/PS1 hippocampal connections. Surprisingly, the I/O relationship and synaptic facilitation were indistinguishable between wild-type (WT) and APP/PS1 connections following IGF-1R blockade. Notably, blockade of other RTK receptors, such as Trks, by K252a inhibitor did not affect synaptic transmission and STP in either WT or APP/PS1 model (Figure S7). These results indicate that enhanced IGF-1R-mediated augmentation of excitatory synaptic transmission may contribute to AD-related hippocampal hyperactivity.

IGF-1R Blockade Increases mEPSC Frequency

As basal IGF-1R activity maintains spike-evoked synaptic transmission, we asked whether it impacts AP-independent quantal synaptic transmission in a similar manner. Therefore, we measured miniature AMPAR-mediated excitatory postsynaptic currents (mEPSCs) using whole-cell voltage-clamp recordings (Figure 6A). Analysis of the mEPSC recordings revealed that the amplitude of mEPSC was not affected by AG1024 (Figures 6B and 6C). Surprisingly, AG1024 induced a pronounced increase

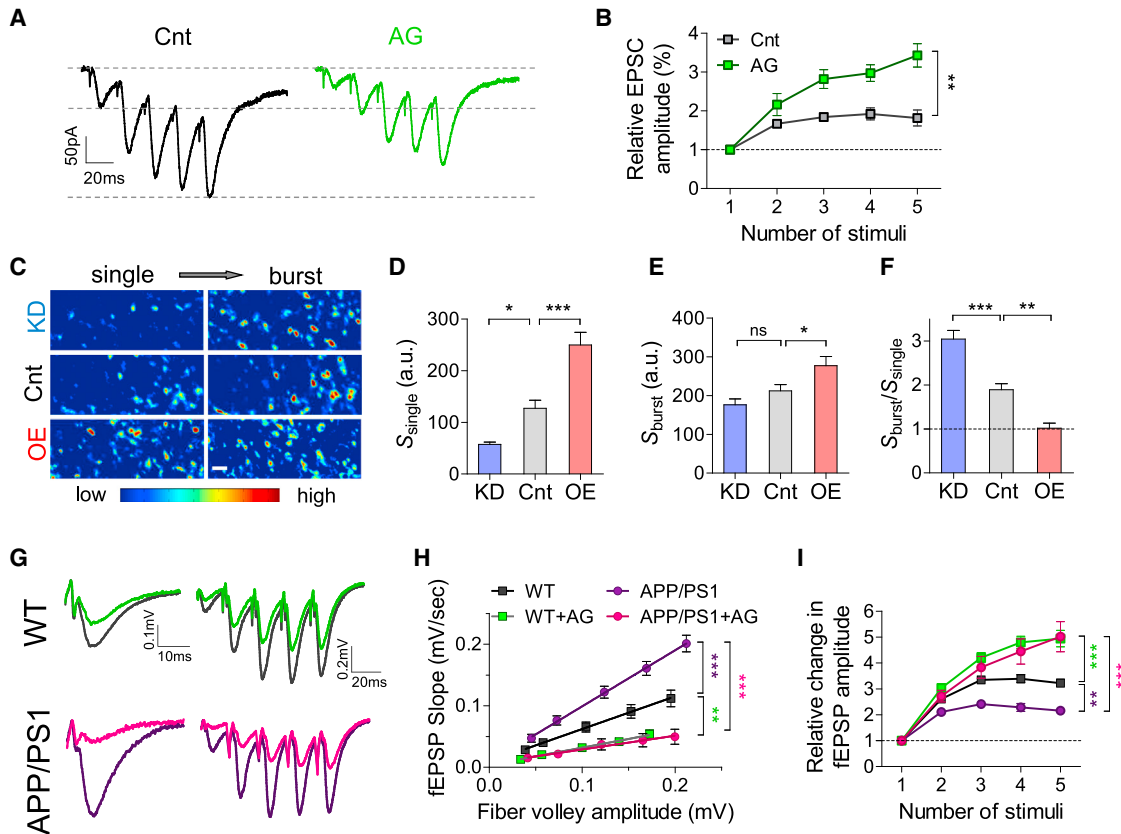


Figure 5. IGF-1R Regulates Short-Term Synaptic Facilitation under Physiological and AD-Related Conditions

(A) Representative recordings of EPSC evoked by bursts (five stimuli at 50 Hz) in acute hippocampal slices before (gray) and 30 min after (green) application of AG1024.
 (B) Relative effect of AG1024 on peak amplitude of each EPSC in the burst normalized to the first EPSC amplitude ($n = 7$).
 (C) Representative ΔF images for single and burst stimulations in hippocampal cultures under control conditions, following IGF-1R KD and IGF-1R overexpression. The scale bar represents $2 \mu\text{m}$.
 (D) During low-frequency stimulation, IGF-1R KD reduced S_{single} ($n = 10$), while IGF1R overexpression increased S_{single} ($n = 10$) compared to control ($n = 8$).
 (E) During high-frequency burst stimulation, IGF-1R KD did not alter S_{burst} ($n = 10$), whereas IGF1R overexpression increased it ($n = 11$) compared to control ($n = 9$).
 (F) IGF-1R KD ($n = 16$) increased STP (two-way ANOVA with post hoc Bonferroni tests) in comparison to control ($n = 10$), while IGF-1R overexpression abolished it ($n = 14$).
 (G) Representative fEPSP recordings evoked by single stimuli and bursts in CA3-CA1 connections of acute slices from WT (top) and APP/PS1 (bottom) mice before and after AG1024 application.
 (H) Higher levels of basal synaptic transmission in APP/PS1 ($n = 13$) compared to WT ($n = 21$) slices as indicated by increased I/O slope. The acute application of $1 \mu\text{M}$ AG1024 (30 min) reduced the I/O slope to the same level in both genotypes.
 (I) Peak amplitude of each fEPSP in the burst normalized to the first fEPSP amplitude. The slices from APP/PS1 ($n = 13$) mice exhibit lower levels of STP compared to WT ones ($n = 19$). The AG1024 increased STP in WT and APP/PS1 mice to the similar level ($*p < 0.05$, $**p < 0.01$, and $***p < 0.001$). The error bars represent SEM.

in mEPSC frequency (2.4-fold; Figures 6D and 6E). These results support differential regulation of the evoked and miniature synaptic vesicle release (Raingo et al., 2012) by basal IGF-1R activity.

IGF-1R Blockade Enhances Resting $[\text{Ca}^{2+}]_{\text{cyto}}$ by Inhibiting $[\text{Ca}^{2+}]_{\text{mito}}$

To understand the dual role of IGF-1R in regulation of spontaneous and evoked vesicle release, we examined the effects of IGF-1R blockade on the cytosolic Ca^{2+} concentration ($[\text{Ca}^{2+}]_{\text{cyto}}$), a critical regulator of vesicle exocytosis. We started from measuring the presynaptic resting $[\text{Ca}^{2+}]_{\text{cyto}}$ using high-affinity fluorescent calcium indicator Oregon Green 488 BAPTA-1

AM (OGB-1 AM) at presynaptic boutons marked by FM4-64 (Figure 7A). IGF1-R blocker AG1024 gradually increased resting Ca^{2+} -dependent fluorescence, reaching the maximal $\sim 40\%$ effect after 25 min from the application (Figures 7B and 7C). This effect was largely blocked by the chelator of intracellular Ca^{2+} , BAPTA-AM (Figure 7B). We next screened for an intracellular source involved in regulation of resting $[\text{Ca}^{2+}]_{\text{cyto}}$. Blockade of sarco/endoplasmic reticulum Ca^{2+} ATPase (SERCA) by thapsigargin or ryanodine receptors by dantrolene did not occlude the effect of AG1024 on resting $[\text{Ca}^{2+}]_{\text{cyto}}$ (Figure 7C). However, blockade of Ca^{2+} uptake by the mitochondrial depolarizing agent carbonyl cyanide *p*-(trifluoromethoxy) phenylhydrazone (FCCP)

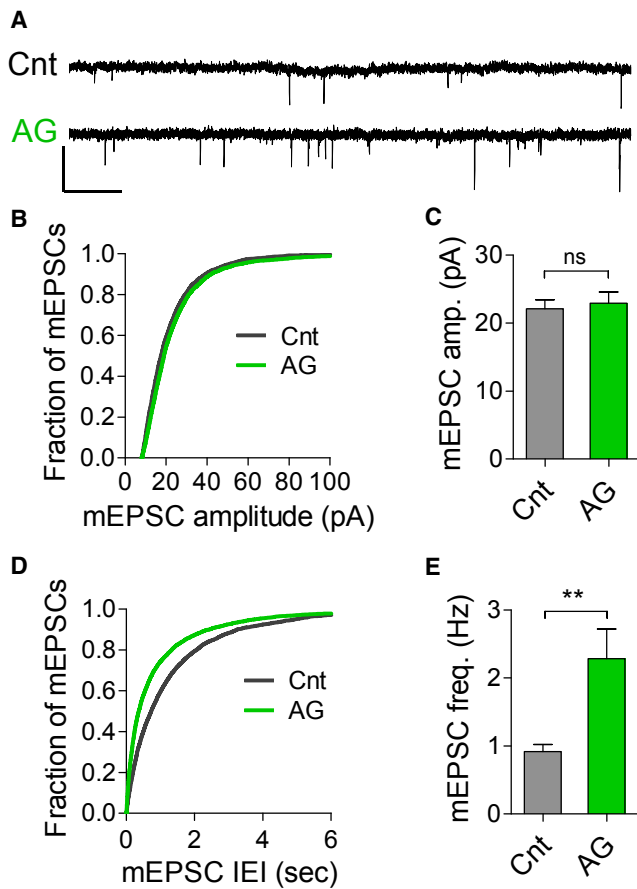


Figure 6. IGF-1R Blockade Increases mEPSC Frequency

(A) Representative traces of mEPSCs for control and following AG1024 application. The scale bars represent 40 pA, 1 s.
 (B) Cumulative histograms of mEPSC amplitudes in control ($n = 21$) and following AG1024 application ($n = 23$).
 (C) Summary of data in (B). The mean of mEPSC amplitude was unaffected by AG1024.
 (D) Cumulative histogram of mEPSC interevent intervals showing a shift to smaller values after IGF-1R blockade (the same experiments as in B).
 (E) Summary of data in (D). The mEPSC frequency is increased 2.5-fold after IGF-1R blockade (** $p < 0.01$ and non-significant, ns). The error bars represent SEM.

(Wang and Thayer, 2002) increased resting $[Ca^{2+}]_{cyto}$ by $\sim 30\%$ and occluded the effect of AG1024 (Figures 7B and 7C). These results point to the mitochondria as a negative regulator of resting $[Ca^{2+}]_{cyto}$ by tonic IGF-1R activity.

To directly assess the effect of IGF-1R tone on mitochondrial Ca^{2+} concentration ($[Ca^{2+}]_{mito}$), we transfected hippocampal neurons with plasmids encoding a highly sensitive genetically encoded Ca^{2+} probe GCaMP6m (Chen et al., 2013), efficiently targeted to mitochondria (2mtGCaMP6m; Patron et al., 2014). The 2mtGCaMP6m co-localized with a mitochondrial marker (mCherry-mito) in hippocampal neurons (Figure 7D). Application of AG1024 inhibited resting $[Ca^{2+}]_{mito}$ (Figure 7E) with a similar kinetics to the increase in the resting $[Ca^{2+}]_{cyto}$ (Figure 7B). FCCP reduced resting $[Ca^{2+}]_{mito}$ and occluded the effect of AG1024 on mitochondrial Ca^{2+} (Figure 7F). Importantly, FCCP enhanced

mEPSC frequency and occluded the effect of AG1024 without altering the mEPSC amplitude (Figure 7G).

As resting $[Ca^{2+}]_{cyto}$ has been shown to inversely correlate with intracellular ATP levels at ribbon synapses (Weiler et al., 2014), we assessed the effect of IGF-1R inhibitor on the presynaptic ATP concentration ($[ATP]_{pre}$). Utilizing a genetically encoded FRET-based ATP reporter that employs the ϵ subunit of the bacterial F_0F_1 -ATP synthase (ATeam1.03; Imamura et al., 2009) fused to a synaptic vesicle protein synaptophysin I (Sypl-ATeam1.03; Shulman et al., 2015), we monitored E_m in the presence of TTX (E_{TTX}) at the presynaptic sites (Figures 7H and 7I). A decrease in E_m reflects reduction in $[ATP]_{pre}$ (Shulman et al., 2015). Resting terminals exhibited a robust E_{TTX} of 0.13 ± 0.005 that was not altered by application of either AG1024 or FCCP or (Figure 7J). Moreover, E_{TTX} was not influenced by mitochondrial ATP synthase inhibitor oligomycin A (Oligo; Figure 7K), while reduced by $\sim 40\%$ by glycolysis blocker 2-deoxyglucose (dGlu; Figure 7K). These results support the conclusion of a recent study that utilized different ATP reporter (Rangaraju et al., 2014) and emphasize that glycolysis, but not mitochondrial function, maintains the presynaptic ATP levels in the absence of spiking activity. Taken together, our data demonstrate that tonic IGF-1R activation inhibits resting $[Ca^{2+}]_{mito}$ without altering $[ATP]_{pre}$ under miniature synaptic activity. Thus, IGF-1R tone regulates both resting $[Ca^{2+}]_{cyto}$ and miniature vesicle release via mitochondrial Ca^{2+} buffering.

IGF-1R Blockade Inhibits $[ATP]_{pre}$ without Altering Ca^{2+}_{mito} during Spiking Activity

Next, we asked whether IGF-1R activity modulates mitochondrial Ca^{2+} transients evoked by APs. Earlier studies using synthetic cationic calcium indicators were able to directly record mitochondrial Ca^{2+} transients evoked by intense stimulations in neuromuscular junction (NMJ) synapses (David et al., 2003) or by high potassium application in cultured forebrain neurons (White and Reynolds, 1995). However, chemical indicators have major drawbacks such as inefficient targeting, uneven distribution of the dye within mitochondria, and potential toxicity (Pozzan and Rudolf, 2009). To examine whether single spikes trigger mitochondrial Ca^{2+} influx, we used a genetically encoded, efficiently targeted to mitochondria 2mtGCaMP6m probe (Patron et al., 2014) with broad dynamic range and high calcium affinity ($K_d = 167$ nM; Chen et al., 2013). Ca^{2+}_{mito} transients were monitored in response to stimulation of hippocampal neurons by single APs or short bursts (5 APs at 100 Hz). Single APs evoked highly heterogeneous responses in both puncta and filament-like mitochondria, giving an average increase of $\sim 8.3\%$ (Figures 8A–8C). The same mitochondria displayed larger ($\sim 33\%$ average peak amplitude), but still variable responses to bursts (Figures 8A–8C). KD of mitochondrial Ca^{2+} uniporter (MCU), an essential component of Ca^{2+} uptake to mitochondria (Baughman et al., 2011; De Stefani et al., 2011), significantly reduced Ca^{2+}_{mito} transients in hippocampal axons (Figures 8C and 8D), confirming the specificity of the 2mtGCaMP6m probe. Application of AG1024 did not affect Ca^{2+}_{mito} transients in response to single or burst stimuli (Figures 8C and 8D).

Since mitochondria is the major source of ATP in neurons (Harris et al., 2012), we next assessed the role of IGF-1Rs in regulation of $[ATP]_{pre}$ under spiking activity. Using a FRET-based

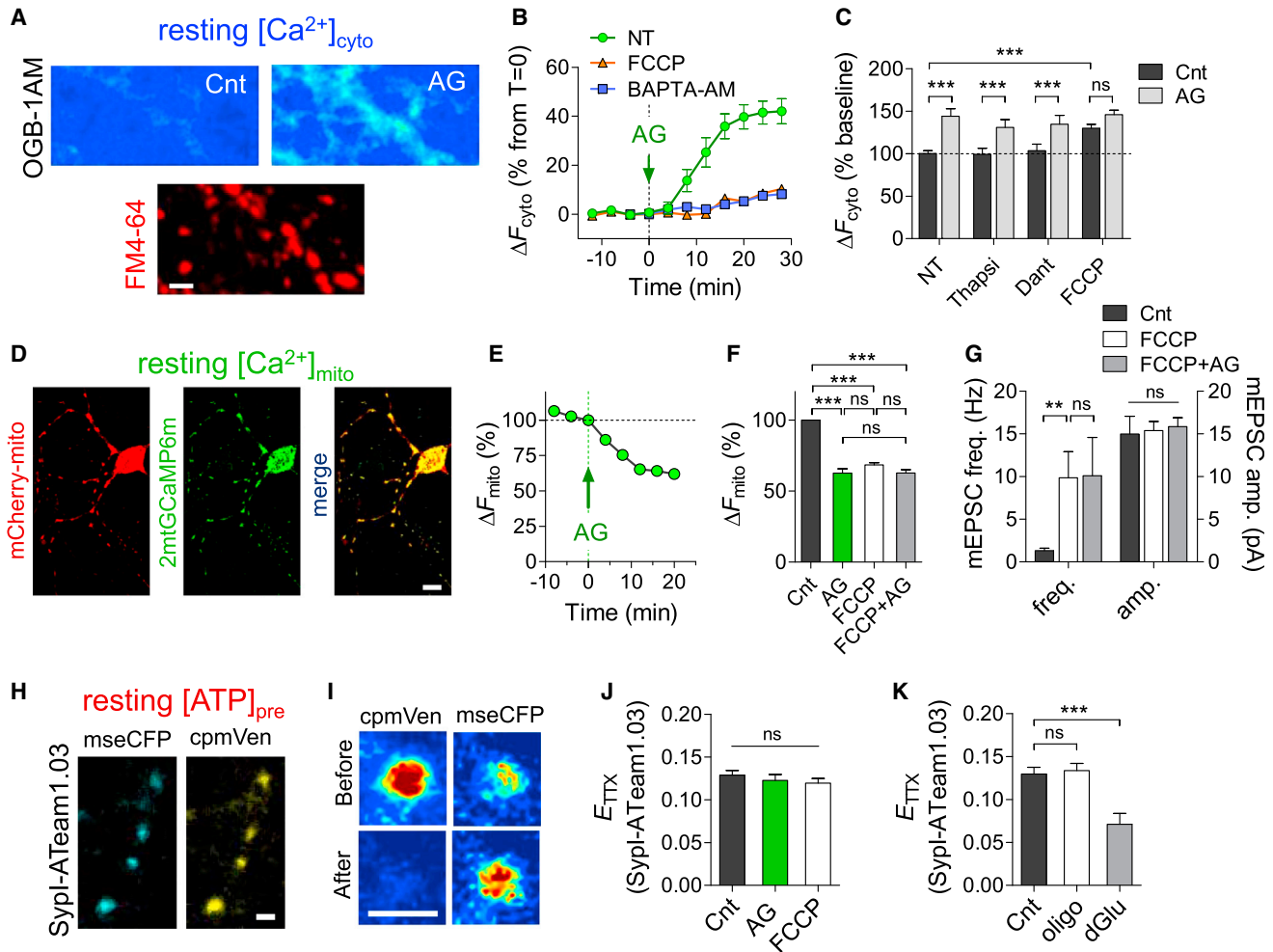


Figure 7. Basal IGF-1R Activity Enhances mEPSC Frequency by Reducing Resting $[Ca^{2+}]_{mito}$

(A) Representative images of OGB-1 AM Ca^{2+} indicator before and 30 min after AG1024 application (top). The FM4-64 dye staining that labels the functional presynaptic boutons in the same area is shown (bottom). The scale bar represents $2 \mu m$.

(B) Time course of AG1024-mediated increase in resting Ca^{2+} at presynaptic boutons under control ($n = 282$), FCCP ($1 \mu M$, 30 min preincubation, and $n = 361$), and BAPTA-AM ($10 \mu M$, 30 min pre incubation, and $n = 198$) conditions.

(C) Summary of AG1024 effect (% of $t = 0$) on resting $[Ca^{2+}]_{cyto}$ at presynaptic boutons under TTX in non-treated (NT, $n = 707$), thapsigargin (Thapsi, $10 \mu M$ and $n = 219$), dantrolene (Dant, $10 \mu M$ and $n = 137$), and FCCP ($1 \mu M$ and $n = 904$) treated cultures. In all the conditions, the blockers were incubated for 30 min prior to AG1024 application.

(D) Representative confocal images of a hippocampal neuron expressing mCherry-mito (left), 2mtGCaMP6m (middle), and the merged image of both markers showing overlapping expression (right). The scale bar represents $10 \mu m$.

(E) Time course of resting $[Ca^{2+}]_{mito}$ following application of AG1024 ($n = 53$).

(F) Summary of AG1024 ($n = 58$), FCCP ($n = 62$), or FCCP+AG ($n = 39$) effects (30 min incubation) on resting $[Ca^{2+}]_{mito}$.

(G) Summary of mEPSC frequency and amplitude under Cnt ($n = 14$), FCCP ($n = 14$), and FCCP+AG ($n = 10$) conditions.

(H) Representative confocal images of boutons of a hippocampal neuron infected with Sypl-A.Team1.03. The scale bar represents $2 \mu m$.

(I) Pseudocolor-coded fluorescence images of mseCFP and cpmVen showing increased cpmVen fluorescence following mseCFP photobleaching. The scale bar represents $2 \mu m$.

(J) E_{TTX} in Cnt ($n = 292$) and following application of AG1024 ($n = 210$) or FCCP ($n = 287$).

(K) E_{TTX} in Cnt ($n = 180$) and following application of oligomycin ($n = 154$) or dGlu ($n = 48$) (** $p < 0.01$ and *** $p < 0.001$) (non-significant, ns). The error bars represent SEM.

reporter of $[ATP]_{pre}$, we found that AG1024 caused a 22% reduction in $[ATP]_{pre}$ during spontaneous spiking activity (Figure 8E). Reduction of $[ATP]_{pre}$ by mitochondrial ATP synthase inhibitor oligomycin or mitochondrial depolarizing agent FCCP occluded the effect of AG1024, indicating that mitochondria mediate the effect

of IGF-1R on presynaptic ATP levels (Figure 8E). It is important to note that inhibition of ATP synthase by oligomycin did not alter spike-evoked Ca^{2+}_{mito} transients (Figures 8C and 8D), while inhibition of Ca^{2+}_{mito} transients by shMCU did not affect $[ATP]_{pre}$ (Figure 8F). Based on these results, we conclude that

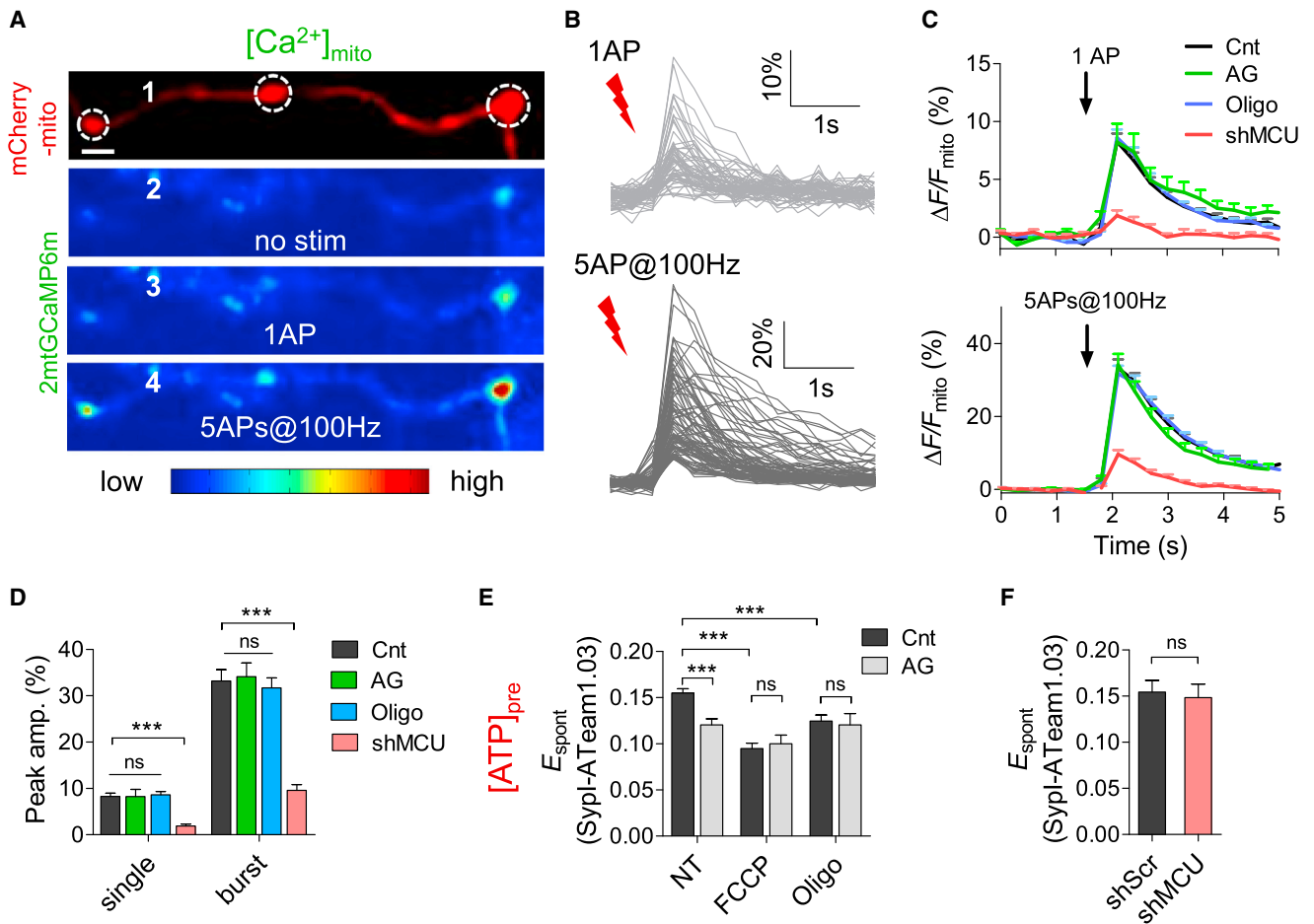


Figure 8. Basal IGF-1R Activity Inhibits AP-Evoked $[ATP]_{pre}$ and Slows Ca^{2+}_{mito} Transients

(A) Representative high-magnification confocal images of an axon of hippocampal neuron expressing mito-tracker (1) and 2mtGCaMP6m without stimulation (2), following single AP (3), and following burst of 5 APs at 100 Hz (4). The scale bar represents 2 μ m.

(B) Traces of Ca^{2+}_{mito} transients at different boutons evoked by single AP at 0.1 Hz (top) or by burst of 5 APs at 100 Hz, inter-burst interval 30 s (bottom), quantified as $\Delta F/F$ (average of ten traces).

(C) Averaged Ca^{2+}_{mito} transients for single (top) or burst (bottom) stimulations under control ($n = 89, 80$), AG1024 (1 μ M and $n = 34, 43$), oligomycin (1 μ g/ml and $n = 96, 94$), and shMCU (65% KD efficiency and $n = 22, 30$) conditions.

(D) Peak amplitude summary of Ca^{2+}_{mito} transients for the data presented in (C).

(E) Effect of AG1024 on E_m under spontaneous spiking activity under non-treated conditions ($n_{cnt} = 431$ and $n_{AG} = 165$), following preincubation with FCCP ($n_{cnt} = 198$ and $n_{AG} = 70$), or oligomycin ($n_{cnt} = 191$ and $n_{AG} = 73$).

(F) shMCU does not affect E_m under spontaneous spiking activity ($n_{shScr} = 75$, $n_{shMCU} = 47$, and $p = 0.77$)

IGF-1R blockade inhibits mitochondrial ATP production without altering Ca^{2+}_{mito} transients under spike-evoked synaptic activity.

Mitochondrial ATP Mediates IGF1R-Induced Presynaptic Modulation

Finally, we asked whether mitochondria mediate modulation of evoked presynaptic Ca^{2+} transients and synaptic vesicle release via IGF-1Rs. AP-evoked presynaptic Ca^{2+}_{cyto} transients were measured using OGB-1 AM at functional boutons marked by FM4-64. While AG1024 increased resting $[Ca^{2+}]_{cyto}$ (Figures 7A–7C), it had an opposite effect on the AP-evoked transients, decreasing the total charge transfer by 46% (Figures 9A, 9B, S8A, and S8B). Similar results were observed by preincubation with PPP inhibitor (Figures S8D–S8F). The reduction in AP-

evoked Ca^{2+}_{cyto} transients by AG1024 was mimicked and occluded by both FCCP and oligomycin (Figures 9A, 9B, S8A, and S8B). It is worth mentioning that oligomycin did not affect resting $[Ca^{2+}]_{cyto}$ (Figure S8C), suggesting that reduction in mitochondrial ATP synthesis, but not an increase in resting $[Ca^{2+}]_{cyto}$, mediates IGF1R-induced inhibition of evoked Ca^{2+} flux. As a consequence of reduction in the presynaptic Ca^{2+} flux, both FCCP and oligomycin inhibited AP-evoked vesicle recycling and occluded the presynaptic effect of AG1024 (Figures 9C and 9D). Moreover, co-application of FCCP and oligomycin in hippocampal slices profoundly inhibited basal CA3-CA1 synaptic transmission and enhanced synaptic facilitation, occluding further effect of AG1024 on these parameters (Figures 9E–9G). Based on these results, we conclude that the IGF-1R tone

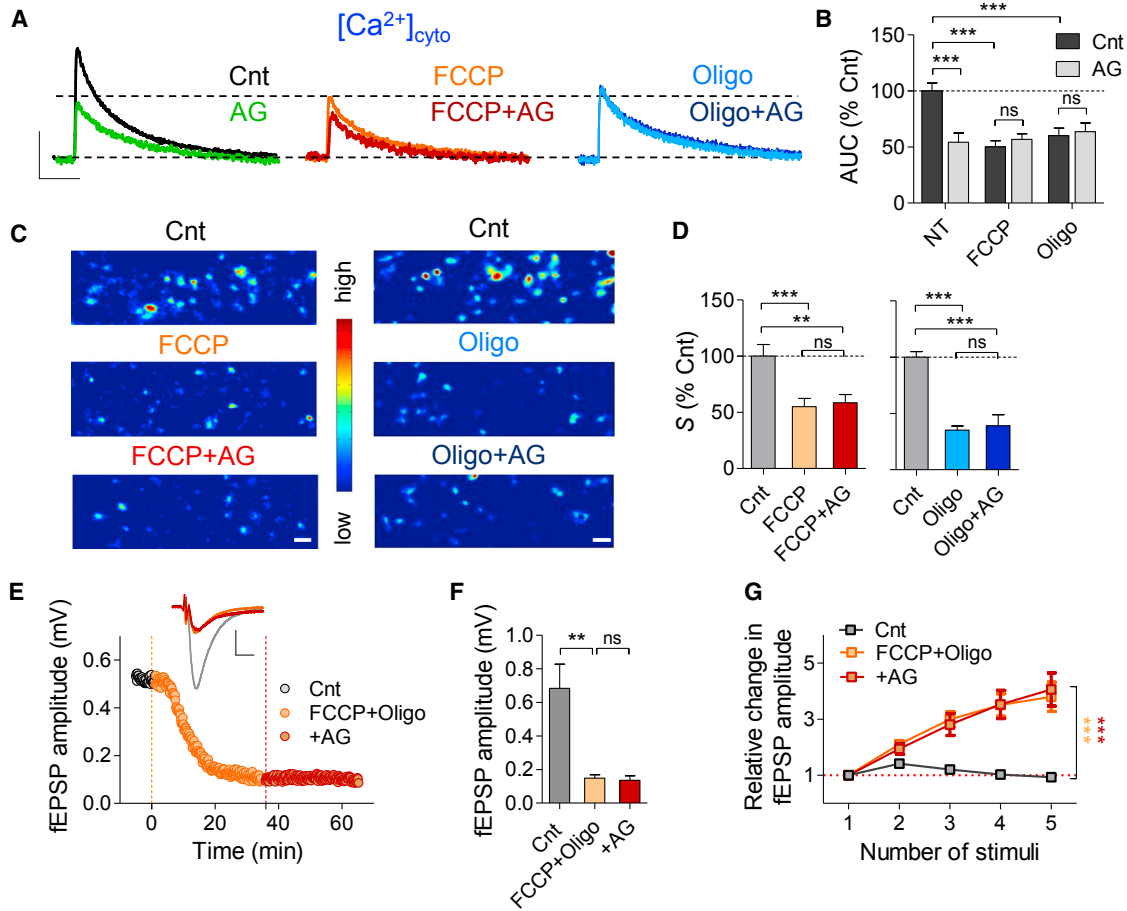


Figure 9. Basal IGF-1R Activity Suppresses AP-Evoked $\text{Ca}^{2+}_{\text{cyto}}$ Transients and Synaptic Vesicle Recycling by Inhibiting Mitochondrial ATP Synthesis

(A) Representative traces of $\text{Ca}^{2+}_{\text{cyto}}$ transients evoked by 0.1 Hz stimulation during 500 Hz line scan at boutons and quantified as $\Delta F/F$ (average of ten traces) showing the effect of AG1024 under non-treated (NT) and in the presence of FCCP or oligomycin. The scale bars represent 20%, 200 ms.

(B) AG1024 reduces the charge transfer of $\text{Ca}^{2+}_{\text{cyto}}$ transients in non-treated conditions ($n_{\text{Cnt}} = 36$ and $n_{\text{AG}} = 32$), but not in the presence of FCCP ($n_{\text{Cnt}} = 28$ and $n_{\text{AG}} = 25$) or oligomycin ($n_{\text{Cnt}} = 23$ and $n_{\text{AG}} = 24$).

(C) Representative color-coded ΔF images showing the effect of AG1024 in FCCP-treated (left) and oligomycin-treated (right) cultures on presynaptic vesicle recycling measured by FM1-43 staining (30 stimuli at 1 Hz).

(D) FCCP ($n = 25$) reduced total S compared to Cnt ($n = 18$) and prevented AG1024 effect ($n = 15$) (left). Oligomycin ($n = 14$) reduced the total S compared to Cnt ($n = 23$) and prevented AG1024 effect ($n = 9$) (right) (** $p < 0.01$ and *** $p < 0.001$). The error bars represent SEM.

(E) Time course of the effect of FCCP and oligomycin on fEPSP amplitude before and after application of AG1024 in CA3-CA1 connections in acute slices. The representative fEPSP recordings evoked by 0.1 Hz stimuli in control (gray), following co-application of 1 μM FCCP and 1 $\mu\text{g/ml}$ oligomycin (orange), and after subsequent 1 μM AG1024 application (brown) (insert). The scale bars represent 0.2 mV, 10 ms.

(F) FCCP and oligomycin reduced fEPSP amplitude and occluded the effect of AG1024 in CA3-CA1 connections ($n = 4$).

(G) FCCP and oligomycin increased short-term facilitation evoked by bursts (five stimuli at 50 Hz) and occluded the effect of AG1024 in CA3-CA1 connections ($n = 4$).

maintains AP-evoked presynaptic Ca^{2+} flux and thus synaptic transmission via mitochondria by preserving presynaptic ATP levels (Figure S9).

DISCUSSION

This study examines the role of endogenously active IGF-1Rs in synaptic vesicle release, synaptic transmission, and STP of hippocampal neurons. Our strategy was to study the functional consequences of the pharmacological blockade or genetic KD of IGF-1Rs in hippocampal circuits. We have employed several ap-

proaches, including intracellular electrophysiology in CA3-CA1 neuronal connections, imaging of synaptic vesicle recycling, and calcium transients in cytosol and mitochondria, together with a FRET-based approach to monitor IGF-1R signaling and ATP levels at synapses. Our results provide converging evidence that the presynaptic IGF-1Rs are basally active, playing a critical role in the maintenance of ongoing neuronal activity. These results are important for several reasons. First, they demonstrate the feasibility of studying IGF-1R signaling at high spatial resolution of single synapses in live neurons. Second, they show that basal IGF-1R activity is critical for maintaining a proper level of

synaptic transmission and ongoing spiking activity. Third, they highlight a critical role of mitochondria in synaptic physiology and its regulation by IGF-1R tone. Fourth, they reveal that IGF-1R activation during high-frequency stimulation modulates synaptic transfer function. Finally, the present data also point to the importance of the IGF-1R signaling in hippocampal hyperactivity under pathological conditions such as AD.

IGF-1Rs Are Basally Active in the Vicinity of Hippocampal Synapses

The binding affinity of IGF-1R toward IGF-1 (0.16 nM; Adams et al., 2000) and the physiological range of the extracellular IGF-1 concentrations in the brain (0.14–0.31 nM; Yamaguchi et al., 1990) imply that IGF-1Rs should be basally activated under spontaneous synaptic activity in hippocampal circuits. As IGF-1R activity can be differentially regulated in various sub-cellular compartments, we applied FRET methodology to estimate IGF-1R activation in the vicinity of synapses by monitoring interactions within the IGF-1R homodimers (Kavran et al., 2014). In addition, we monitored local activity of the downstream signaling molecule Akt. The following facts suggest that the presynaptic IGF-1Rs are activated by the extracellular IGF-1: First, activation of the IGF-1R and its downstream signaling can be reduced by pharmacological IGF-1R inhibition or genetic IGF-1R KD, while unaffected by IGF-1 application. Second, KD of IGF-1 ligand reduces both IGF-1R activity and synaptic vesicle exocytosis. Importantly, ectopically applied IGF-1 rescues shIGF1-induced reduction in IGF-1R activity and *Pr*. These data indicate that the presynaptic IGF-1Rs are largely occupied by the extracellular IGF-1 during spontaneous synaptic activity. Thus, upregulation of the IGF-1R expression appears to be a more relevant mechanism to augment presynaptic IGF-1R tone.

IGF-1R and Synaptic Function

Temporally, IGF-1Rs may act within minutes to modify synaptic function, over hours and days to alter gene expression and neuronal structures, and months to regulate brain growth. While extensive studies demonstrate a key role of IGF-1Rs in neuronal growth and development, whether IGF-1Rs directly regulate information processing at short timescales remains obscure. Our experiments demonstrate that blockade of IGF-1Rs induces an increase in resting Ca^{2+} levels and spontaneous vesicle release, while inhibiting AP-evoked Ca^{2+} transients and evoked vesicle release. This suggests that basal IGF-1R activity promotes evoked synaptic transmission, while functions as a suppressor of spontaneous transmission. Originally dismissed as synaptic noise, recent evidence suggests that synapses use physically segregated pathways to decode spontaneous and evoked neurotransmission (Atasoy et al., 2008; Peled et al., 2014) and that these two types of transmission could have specialized physiological roles (Ramirez and Kavalali, 2011).

How typical is IGF-1R function among other RTKs expressed in the hippocampus? While both IGF-1Rs and TrkB receptors (TrkBRS) potentiate evoked excitatory synaptic transmission, their rapid effects are associated with different types of neuronal activity. Brain-derived neurotrophic factor (BDNF) requires presynaptic depolarization in order to efficiently potentiate synaptic strength via TrkBRS (Boulanger and Poo, 1999; Slutsky et al., 2004) and mediates persistent potentiation induced by theta-

bursts (Kang et al., 1997). Moreover, blockade of TrkBRS does not alter either basal synaptic transmission or short-term synaptic plasticity (Figure S7; Kang et al., 1997), indicating that TrkBRS are not activated by basal BDNF levels in hippocampal circuits. These findings suggest that TrkBRS may rapidly regulate synaptic transmission, which is temporally locked to high-frequency discharges of afferent inputs or coincidence detection of pre and postsynaptic spikes. Conversely, extracellular IGF-1 activates IGF-1Rs under resting conditions, maintaining basal transmission and ongoing spiking activity in the physiological range, while suppressing background miniature synaptic activity (Figure S9). Thus, two key RTKs—IGF-1R and TrkBRS—differentially regulate information processing in hippocampal circuits.

Mitochondrion as a Dual Regulator of Synaptic Vesicle Release

Early studies demonstrate heterogeneous data on the role of mitochondria in regulation of spontaneous synaptic vesicle release: mitochondrial inhibitors produced an increase in the rate of spontaneous synaptic transmission in hippocampal neurons (Scotti et al., 1999) and in the frog NMJ (Alnaes and Rahamimoff, 1975). However, genetic deletion of mitochondria from synaptic sites of *Drosophila* NMJ produced a non-robust increase in miniature transmission, despite a 2-fold increase in resting $[Ca^{2+}]_{cyto}$ (Verstreken et al., 2005) or an increase in spontaneous transmission in less than half of mutant muscles (Guo et al., 2005). Furthermore, the role of mitochondria in short-term synaptic plasticity also remains controversial: mitochondrial Ca^{2+} buffering was implicated in some studies (Billups and Forsythe, 2002; David et al., 2003; Tang and Zucker, 1997), while mitochondrial ATP production in others (Guo et al., 2005; Verstreken et al., 2005). Thus, differences in the relationships between presynaptic VGCCs, mitochondrial Ca^{2+} buffering, and ATP production may underlie heterogeneous impact of mitochondria on synaptic vesicle exocytosis at various types of synapses.

Utilizing recently developed genetically encoded Ca^{2+} and ATP sensors, we were able to distinguish between two mitochondrial functions— Ca^{2+} buffering and ATP production—at the level of single synapses. We found that presynaptic IGF-1Rs differentially regulate Ca^{2+}_{mito} and ATP levels during periods of miniature and spike-evoked vesicle release. On the one hand, IGF-1R blockade decreases resting $[Ca^{2+}]_{mito}$ without altering $[ATP]_{pre}$ in the absence of spikes. On the other hand, IGF-1R blockade lowers $[ATP]_{pre}$ without altering Ca^{2+}_{mito} transients during spiking activity. As a result, IGF-1R tone constrains resting $[Ca^{2+}]_{cyto}$ and spontaneous vesicle release, while maintaining AP-evoked presynaptic Ca^{2+} transients and *Pr* during spiking activity. It is worth mentioning that we monitored global ATP and Ca^{2+} levels at the presynaptic sites. However, local ATP and Ca^{2+} changes in the vicinity of VGCCs might be much higher due to a close proximity of VGCCs and mitochondria (Rizzuto et al., 2012), thus significantly impacting vesicle exocytosis. ATP may maintain evoked presynaptic Ca^{2+} transients by stabilizing VGCC and reducing its rundown (Wu et al., 2002) or by regulating membrane depolarization via ATP-sensitive potassium (K_{ATP}) channels (Koster et al., 2005). Regardless of the precise molecular mechanism, IGF-1R tone maintains evoked-to-spontaneous transmission ratio by controlling two separate mitochondrial functions: Ca^{2+} buffering and energy supply.

IGF-1R and AD-Associated Synaptic Dysfunctions

The role of IGF-1Rs in neurodegenerative disorders has remained highly controversial. While IGF-1 injections promote A β clearance (Carro et al., 2002) and blockade of IGF-1Rs in the choroid plexus exacerbate AD-like pathology, genetic reduction in the IGF-1R protects mice from A β -associated proteotoxicity (Cohen et al., 2009; Freude et al., 2009). Our study suggests that IGF-1R overexpression, observed in the hippocampus of APP/PS1 mice (Zhang et al., 2013), triggers presynaptic dysfunctions at the early stage, preceding synaptic loss and A β aggregation. Namely, increase in the IGF-1R-mediated synaptic modulation contributes to augmented basal synaptic transmission and reduced STP in CA3-CA1 hippocampal connections of young APP/PS1 mice. Our results propose that inhibition of IGF-1Rs may reduce AD-associated hippocampal hyperactivity at the early stages of AD progression. It remains to be seen whether IGF-1R inhibition may reverse hippocampal hyperactivity in people who are at risk for AD and AD patients (Bakker et al., 2012; Vossel et al., 2013).

EXPERIMENTAL PROCEDURES

Primary Hippocampal Cultures and Acute Hippocampal Slices

All animal experiments were approved by the Tel Aviv University Committee on Animal Care. Primary cultures of CA3-CA1 hippocampal neurons were prepared from WT mice (BALB/c background) on postnatal days 0–2 as described (Slutsky et al., 2004). Acute hippocampal slices were prepared from 2-month-old BALB/c, APP^{swe}/PS1^{dE9} (Jankowsky et al., 2004), and the corresponding WT (B6C3F1/J background) mice. All animals were kept in a normal light/dark cycle (12 hr/12 hr), three animals per cage. Coronal slices (400 μ m for extracellular recordings and 350 μ m for intracellular patch recordings) of hippocampus were prepared as described before (Abramov et al., 2009). Slices were transferred to a submerged recovery chamber at room temperature containing oxygenated (95% O₂ and 5% CO₂) artificial cerebrospinal fluid (ACSF) for 1 hr before the experiment. The ACSF contained, in mM: NaCl, 125; KCl, 2.5; CaCl₂, 1.2; MgCl₂, 1.2; NaHCO₃, 25; NaH₂PO₄, 1.25; and glucose, 25.

Plasmids, Transfection, Infection

AktAR (Cer-FHA1-FOXO-cpVE172) FRET construct (Gao and Zhang, 2008) was a gift of Dr. Zhang (John Hopkins University); Sypl-A^{Team1.03} (Shulman et al., 2015) of Dr. Daniel Gitler (Ben-Gurion University); 2mtGCamp6m of Dr. Diego De Stefani (University of Padova), and mCherry-mito of Dr. Israel Sekler (Ben-Gurion University). Human IGF-1R^{Civ/Cer} was constructed and expressed in pEGFP-N1 based vector under control of cytomegalovirus (CMV) promoter.

For shRNA-mediated KD, we used the following plasmids: for IGF-1R KD - SHCLNG-NM_010513 plasmid (Sigma-Aldrich, catalog number TRCN0000023493, clone ID: NM_010513.1-3656s1c1 and TRCN0000023489, clone ID: NM_010513.1-487s1c1); for IGF-1 KD - SHCLNG-NM_010512 (Sigma-Aldrich, catalog number TRCN0000066354, clone ID: NM_010512.2-354s1c1); and for MCU KD - SHCLNG-NM_001033259 (Sigma-Aldrich, catalog number TRCN0000251263, clone ID: NM_001033259.3-1211s21c1).

Transient cDNA transfections were performed using Lipofectamine-2000 reagents and neurons were typically imaged 18–24 hr after transfection. Infections with lentivirus (LVs) were done at DIV6 and the experiments were performed at >DIV14.

STED Microscopy

Dual-color STED microscopy was performed using a STED microscope (TCS SP5, Leica) as described before (Revelo et al., 2014). The cells were stained for IGF-1R (Cell Signaling, #3027), synaptophysin (Synaptic Systems, #101 011), and Homer 1 (Synaptic Systems, #160 011), and were labeled using Chromo494 or ATTO647N coupled secondary antibodies.

Confocal Imaging in Primary Hippocampal Cultures

The experiments were performed in mature (15–28 days in vitro) cultures. Hippocampal neurons were imaged using a FV1000 spectral Olympus confocal microscope using a 60 \times 1.2 NA water-immersion objective. The experiments were conducted at room temperature in extracellular Tyrode solution containing 145 mM NaCl, 3 mM KCl, 15 mM glucose, 10 mM HEPES, 1.2 mM MgCl₂, 1.2 mM CaCl₂, and pH adjusted to 7.4 with NaOH.

For FM-based imaging and analysis, activity-dependent FM1-43 (10 μ M) and FM4-64 (15 μ M) styryl dyes were used to estimate basal synaptic vesicle recycling and exocytosis using protocols described previously (Abramov et al., 2009).

For monitoring presynaptic cytosolic Ca²⁺ transients, fluorescent calcium indicator OGB-1 AM was used. For detection of Ca²⁺ transients in mitochondria, neurons were co-transfected with 2mtGCamp6m and mCherry-mito.

For FRET imaging and analysis, images were 512 \times 512 pixels, with a pixel width of 92–110 nm. Intensity-based FRET imaging and analysis was carried as described before (Laviv et al., 2010).

Electrophysiology

Experiments were performed at room temperature. EPSCs and fEPSPs were recorded in acute hippocampal slices with a glass pipette containing Tyrode solution (1–2 M Ω) from synapses in the CA1 stratum radiatum using a Multi-Clamp 700B amplifier (Molecular Devices). Stimulation of the SC pathway was delivered through a glass suction electrode (10–20 μ m tip) filled with Tyrode. For mEPSCs recordings in hippocampal cultures, TTX (1 μ M), amino-phosphonopentanoate (AP-5; 50 μ M), and gabazine (30 μ M) were added to Tyrode solution. EPSCs and mEPSCs were recorded using the following intracellular solution: 120 mM Cs-MeSO₃, 10 mM HEPES, 10 mM NaCl, 0.5 mM CaCl₂, 2 mM Mg²⁺-ATP, 0.3 mM Na₃GTP, 10 mM EGTA, and pH adjusted to 7.25 with NaOH. Recordings with access resistances that exceeded 20 M Ω (for evoked EPSCs) or 10 M Ω (for mEPSCs) or that varied by >20% were excluded from analysis. Serial resistance was not compensated. Data were analyzed using Mini Analysis (Synaptosoft) for mEPSCs and in pCLAMP 10 (Molecular Devices) for EPSCs and fEPSPs.

Statistical Analysis

One-way ANOVA analysis with post hoc Bonferroni's were used to compare several conditions. Two-way ANOVA with post hoc Bonferroni's were used to compare short-term synaptic plasticity during burst of five stimuli under different conditions. Unpaired two-tailed t tests were used for two-group comparison. Nonparametric Spearman test has been used for correlation analysis. N is designated for the number of neurons in patch clamp experiments, slices in field recordings, and number of synapses in imaging experiments (each experimental condition was repeated at least in three different mice/batches of cultures) (*p < 0.05; **p < 0.01; and ***p < 0.001).

For the detailed description of the procedures, see [Supplemental Information](#).

SUPPLEMENTAL INFORMATION

Supplemental Information includes Supplemental Experimental Procedures and nine figures and can be found with this article online at <http://dx.doi.org/10.1016/j.neuron.2015.12.034>.

AUTHOR CONTRIBUTIONS

Conceptualization, I. Slutsky and N.G.; Methodology, I. Slutsky, N.G., and S.R.; Investigation, N.G., I.V., M.H., E.S., I. Shapiro, M.S., and Y.M.; Writing, I. Slutsky and N.G. with input from all authors; Funding acquisition, I. Slutsky and S.R.; and Supervision, I. Slutsky. This work was performed in partial fulfillment of the requirements for a Ph.D. degree by N.G. at the Sackler Faculty of Medicine and Sagol School of Neuroscience, Tel Aviv University, Israel.

ACKNOWLEDGMENTS

We thank Ehud Cohen, Israel Sekler, Daniel Khananshvil, Rive Sarfstein, and Haim Werner for discussions; Nir Ofir for help with data analysis; Samuel Frere

and Hila Milshtein for comments on the manuscript; Yevgeny Berdichevsky for IGF-1R^{Cit/Cer}; Daniel Gitler for Sypl-ATeam1.03; Diego De Stefani for 2mtGCAMP6m; Israel Sekler for mCherry-mito; Fabiana Perocchi for shMCU; and Yoav Ben-Simon for shScr. This work was supported by the European Research Council starting grant (281403, I. Slutsky), the Legacy Heritage Biomedical Program of the Israel Science Foundation (1195/14, I. Slutsky), Israel Science Foundation (398/13, I. Slutsky), Binational Science Foundation (2013244, I. Slutsky), and the European Research Council (ERC-2013-CoG NeuroMolAnatomy, S.R.). I. Slutsky is grateful to Sheila and Denis Cohen Charitable Trust and Rosetrees Trust of the UK for their support. N.G. is grateful to Sagol School of Neuroscience of Tel Aviv University for the award of doctoral fellowship.

Received: December 13, 2014

Revised: November 19, 2015

Accepted: December 13, 2015

Published: January 21, 2016

REFERENCES

- Abramov, E., Dolev, I., Fogel, H., Ciccotosto, G.D., Ruff, E., and Slutsky, I. (2009). Amyloid-beta as a positive endogenous regulator of release probability at hippocampal synapses. *Nat. Neurosci.* *12*, 1567–1576.
- Adams, T.E., Epa, V.C., Garrett, T.P.J., and Ward, C.W. (2000). Structure and function of the type 1 insulin-like growth factor receptor. *Cell. Mol. Life Sci.* *57*, 1050–1093.
- Alnaes, E., and Rahamimoff, R. (1975). On the role of mitochondria in transmitter release from motor nerve terminals. *J. Physiol.* *248*, 285–306.
- Amaducci, L., and Tesco, G. (1994). Aging as a major risk for degenerative diseases of the central nervous system. *Curr. Opin. Neurol.* *7*, 283–286.
- Atasoy, D., Ertunc, M., Moulder, K.L., Blackwell, J., Chung, C., Su, J., and Kavalali, E.T. (2008). Spontaneous and evoked glutamate release activates two populations of NMDA receptors with limited overlap. *J. Neurosci.* *28*, 10151–10166.
- Bakker, A., Krauss, G.L., Albert, M.S., Speck, C.L., Jones, L.R., Stark, C.E., Yassa, M.A., Bassett, S.S., Shelton, A.L., and Gallagher, M. (2012). Reduction of hippocampal hyperactivity improves cognition in amnesic mild cognitive impairment. *Neuron* *74*, 467–474.
- Baughman, J.M., Perocchi, F., Girgis, H.S., Plovanich, M., Belcher-Timme, C.A., Sancak, Y., Bao, X.R., Strittmatter, L., Goldberger, O., Bogorad, R.L., et al. (2011). Integrative genomics identifies MCU as an essential component of the mitochondrial calcium uniporter. *Nature* *476*, 341–345.
- Billups, B., and Forsythe, I.D. (2002). Presynaptic mitochondrial calcium sequestration influences transmission at mammalian central synapses. *J. Neurosci.* *22*, 5840–5847.
- Blair, L.A.C., and Marshall, J. (1997). IGF-1 modulates N and L calcium channels in a PI 3-kinase-dependent manner. *Neuron* *19*, 421–429.
- Boulanger, L.M., and Poo, M.M. (1999). Presynaptic depolarization facilitates neurotrophin-induced synaptic potentiation. *Nat. Neurosci.* *2*, 346–351.
- Cao, P., Maximov, A., and Südhof, T.C. (2011). Activity-dependent IGF-1 exocytosis is controlled by the Ca(2+)-sensor synaptotagmin-10. *Cell* *145*, 300–311.
- Carro, E., Trejo, J.L., Gomez-Isla, T., LeRoith, D., and Torres-Aleman, I. (2002). Serum insulin-like growth factor I regulates brain amyloid-beta levels. *Nat. Med.* *8*, 1390–1397.
- Carro, E., Trejo, J.L., Spuch, C., Bohl, D., Heard, J.M., and Torres-Aleman, I. (2006). Blockade of the insulin-like growth factor I receptor in the choroid plexus originates Alzheimer's-like neuropathology in rodents: new cues into the human disease? *Neurobiol. Aging* *27*, 1618–1631.
- Chen, T.-W., Wardill, T.J., Sun, Y., Pulver, S.R., Renninger, S.L., Baohan, A., Schreier, E.R., Kerr, R.A., Orger, M.B., Jayaraman, V., et al. (2013). Ultrasensitive fluorescent proteins for imaging neuronal activity. *Nature* *499*, 295–300.
- Cohen, E., and Dillin, A. (2008). The insulin paradox: aging, proteotoxicity and neurodegeneration. *Nat. Rev. Neurosci.* *9*, 759–767.
- Cohen, E., Paulsson, J.F., Blinder, P., Burstyn-Cohen, T., Du, D., Estepa, G., Adame, A., Pham, H.M., Holzenberger, M., Kelly, J.W., et al. (2009). Reduced IGF-1 signaling delays age-associated proteotoxicity in mice. *Cell* *139*, 1157–1169.
- D'Ercole, A.J., Ye, P., Calikoglu, A.S., and Gutierrez-Ospina, G. (1996). The role of the insulin-like growth factors in the central nervous system. *Mol. Neurobiol.* *13*, 227–255.
- David, G., Talbot, J., and Barrett, E.F. (2003). Quantitative estimate of mitochondrial [Ca²⁺] in stimulated motor nerve terminals. *Cell Calcium* *33*, 197–206.
- De Stefani, D., Raffaello, A., Teardo, E., Szabò, I., and Rizzuto, R. (2011). A forty-kilodalton protein of the inner membrane is the mitochondrial calcium uniporter. *Nature* *476*, 336–340.
- Ding, Q., Vaynman, S., Akhavan, M., Ying, Z., and Gomez-Pinilla, F. (2006). Insulin-like growth factor I interfaces with brain-derived neurotrophic factor-mediated synaptic plasticity to modulate aspects of exercise-induced cognitive function. *Neuroscience* *140*, 823–833.
- Dobrunz, L.E., and Stevens, C.F. (1997). Heterogeneity of release probability, facilitation, and depletion at central synapses. *Neuron* *18*, 995–1008.
- Dolev, I., Fogel, H., Milshtein, H., Berdichevsky, Y., Lipstein, N., Brose, N., Gazit, N., and Slutsky, I. (2013). Spike bursts increase amyloid-β 40/42 ratio by inducing a presenilin-1 conformational change. *Nat. Neurosci.* *16*, 587–595.
- Fernandez, A.M., and Torres-Aleman, I. (2012). The many faces of insulin-like peptide signalling in the brain. *Nat. Rev. Neurosci.* *13*, 225–239.
- Flier, J.S., Usher, P., and Moses, A.C. (1986). Monoclonal antibody to the type I insulin-like growth factor (IGF-I) receptor blocks IGF-I receptor-mediated DNA synthesis: clarification of the mitogenic mechanisms of IGF-I and insulin in human skin fibroblasts. *Proc. Natl. Acad. Sci. USA* *83*, 664–668.
- Freude, S., Hettich, M.M., Schumann, C., Stöhr, O., Koch, L., Köhler, C., Udelhoven, M., Leiser, U., Müller, M., Kubota, N., et al. (2009). Neuronal IGF-1 resistance reduces Aβ accumulation and protects against premature death in a model of Alzheimer's disease. *FASEB J.* *23*, 3315–3324.
- Gao, X., and Zhang, J. (2008). Spatiotemporal analysis of differential Akt regulation in plasma membrane microdomains. *Mol. Biol. Cell* *19*, 4366–4373.
- Gontier, G., George, C., Chaker, Z., Holzenberger, M., and Aïd, S. (2015). Blocking IGF signaling in adult neurons alleviates Alzheimer's disease pathology through amyloid-β clearance. *J. Neurosci.* *35*, 11500–11513.
- Guo, X., Macleod, G.T., Wellington, A., Hu, F., Panchumarthi, S., Schoenfield, M., Marin, L., Charlton, M.P., Atwood, H.L., and Zinsmaier, K.E. (2005). The GTPase dMiro is required for axonal transport of mitochondria to *Drosophila* synapses. *Neuron* *47*, 379–393.
- Harris, J.J., Jolivet, R., and Attwell, D. (2012). Synaptic energy use and supply. *Neuron* *75*, 762–777.
- Imamura, H., Nhat, K.P., Togawa, H., Saito, K., Iino, R., Kato-Yamada, Y., Nagai, T., and Noji, H. (2009). Visualization of ATP levels inside single living cells with fluorescence resonance energy transfer-based genetically encoded indicators. *Proc. Natl. Acad. Sci. USA* *106*, 15651–15656.
- Jankowsky, J.L., Fadale, D.J., Anderson, J., Xu, G.M., Gonzales, V., Jenkins, N.A., Copeland, N.G., Lee, M.K., Younkin, L.H., Wagner, S.L., et al. (2004). Mutant presenilins specifically elevate the levels of the 42 residue beta-amyloid peptide in vivo: evidence for augmentation of a 42-specific gamma secretase. *Hum. Mol. Genet.* *13*, 159–170.
- Kang, H., Welcher, A.A., Shelton, D., and Schuman, E.M. (1997). Neurotrophins and time: different roles for TrkB signaling in hippocampal long-term potentiation. *Neuron* *19*, 653–664.
- Kar, S., Chabot, J.G., and Quirion, R. (1993). Quantitative autoradiographic localization of [125I]insulin-like growth factor I, [125I]insulin-like growth factor II, and [125I]insulin receptor binding sites in developing and adult rat brain. *J. Comp. Neurol.* *333*, 375–397.
- Kavran, J.M., McCabe, J.M., Byrne, P.O., Connacher, M.K., Wang, Z., Ramek, A., Sarabipour, S., Shan, Y., Shaw, D.E., Hristova, K., et al. (2014). How IGF-1 activates its receptor. *eLife* *3*, 3.

- Kenyon, C.J. (2010). The genetics of ageing. *Nature* *464*, 504–512.
- Koster, J.C., Permutt, M.A., and Nichols, C.G. (2005). Diabetes and insulin secretion: the ATP-sensitive K⁺ channel (K_{ATP}) connection. *Diabetes* *54*, 3065–3072.
- Landi, S., Ciucci, F., Maffei, L., Berardi, N., and Cenni, M.C. (2009). Setting the pace for retinal development: environmental enrichment acts through insulin-like growth factor 1 and brain-derived neurotrophic factor. *J. Neurosci.* *29*, 10809–10819.
- Laviv, T., Riven, I., Dolev, I., Vertkin, I., Balana, B., Slesinger, P.A., and Slutsky, I. (2010). Basal GABA regulates GABA(B)R conformation and release probability at single hippocampal synapses. *Neuron* *67*, 253–267.
- Lemmon, M.A., and Schlessinger, J. (2010). Cell signaling by receptor tyrosine kinases. *Cell* *141*, 1117–1134.
- LeRoith, D., Werner, H., Beitner-Johnson, D., and Roberts, C.T., Jr. (1995). Molecular and cellular aspects of the insulin-like growth factor I receptor. *Endocr. Rev.* *16*, 143–163.
- Moloney, A.M., Griffin, R.J., Timmons, S., O'Connor, R., Ravid, R., and O'Neill, C. (2010). Defects in IGF-1 receptor, insulin receptor and IRS-1/2 in Alzheimer's disease indicate possible resistance to IGF-1 and insulin signaling. *Neurobiol. Aging* *31*, 224–243.
- Párrizas, M., Gazit, A., Levitzki, A., Wertheimer, E., and LeRoith, D. (1997). Specific inhibition of insulin-like growth factor-1 and insulin receptor tyrosine kinase activity and biological function by tyrphostins. *Endocrinology* *138*, 1427–1433.
- Patron, M., Checchetto, V., Raffaello, A., Teardo, E., Vecellio Reane, D., Mantoan, M., Granatiero, V., Szabó, I., De Stefani, D., and Rizzuto, R. (2014). MICU1 and MICU2 finely tune the mitochondrial Ca²⁺ uniporter by exerting opposite effects on MCU activity. *Mol. Cell* *53*, 726–737.
- Peled, E.S., Newman, Z.L., and Isacoff, E.Y. (2014). Evoked and spontaneous transmission favored by distinct sets of synapses. *Curr. Biol.* *24*, 484–493.
- Poo, M.M. (2001). Neurotrophins as synaptic modulators. *Nat. Rev. Neurosci.* *2*, 24–32.
- Pozzan, T., and Rudolf, R. (2009). Measurements of mitochondrial calcium in vivo. *Biochim. Biophys. Acta. Bioenergetics* *1787*, 1317–1323.
- Raino, J., Khvotchev, M., Liu, P., Darios, F., Li, Y.C., Ramirez, D.M., Adachi, M., Lemieux, P., Toth, K., Davletov, B., and Kavalali, E.T. (2012). VAMP4 directs synaptic vesicles to a pool that selectively maintains asynchronous neurotransmission. *Nat. Neurosci.* *15*, 738–745.
- Ramirez, D.M., and Kavalali, E.T. (2011). Differential regulation of spontaneous and evoked neurotransmitter release at central synapses. *Curr. Opin. Neurobiol.* *21*, 275–282.
- Ramsey, M.M., Adams, M.M., Ariwodola, O.J., Sonntag, W.E., and Weiner, J.L. (2005). Functional characterization of des-IGF-1 action at excitatory synapses in the CA1 region of rat hippocampus. *J. Neurophysiol.* *94*, 247–254.
- Rangaraju, V., Calloway, N., and Ryan, T.A. (2014). Activity-driven local ATP synthesis is required for synaptic function. *Cell* *156*, 825–835.
- Revelo, N.H., Kamin, D., Truckenbrodt, S., Wong, A.B., Reuter-Jessen, K., Reisinger, E., Moser, T., and Rizzoli, S.O. (2014). A new probe for super-resolution imaging of membranes elucidates trafficking pathways. *J. Cell Biol.* *205*, 591–606.
- Rizzuto, R., De Stefani, D., Raffaello, A., and Mammucari, C. (2012). Mitochondria as sensors and regulators of calcium signalling. *Nat. Rev. Mol. Cell Biol.* *13*, 566–578.
- Schumacher, R., Mosthaf, L., Schlessinger, J., Brandenburg, D., and Ullrich, A. (1991). Insulin and insulin-like growth factor-1 binding specificity is determined by distinct regions of their cognate receptors. *J. Biol. Chem.* *266*, 19288–19295.
- Scotti, A.L., Chatton, J.Y., and Reuter, H. (1999). Roles of Na⁺-Ca²⁺ exchange and of mitochondria in the regulation of presynaptic Ca²⁺ and spontaneous glutamate release. *Philos. Trans. R. Soc. Lond. B Biol. Sci.* *354*, 357–364.
- Shulman, Y., Stavsky, A., Fedorova, T., Mikulincer, D., Atias, M., Radinsky, I., Kahn, J., Slutsky, I., and Gitler, D. (2015). ATP binding to synapsin IIa regulates usage and clustering of vesicles in terminals of hippocampal neurons. *J. Neurosci.* *35*, 985–998.
- Slutsky, I., Sadeghpour, S., Li, B., and Liu, G. (2004). Enhancement of synaptic plasticity through chronically reduced Ca²⁺ flux during uncorrelated activity. *Neuron* *44*, 835–849.
- Suh, Y., Atzmon, G., Cho, M.-O., Hwang, D., Liu, B., Leahy, D.J., Barzilai, N., and Cohen, P. (2008). Functionally significant insulin-like growth factor I receptor mutations in centenarians. *Proc. Natl. Acad. Sci. USA* *105*, 3438–3442.
- Tang, Y., and Zucker, R.S. (1997). Mitochondrial involvement in post-tetanic potentiation of synaptic transmission. *Neuron* *18*, 483–491.
- Trejo, J.L., Carro, E., and Torres-Aleman, I. (2001). Circulating insulin-like growth factor I mediates exercise-induced increases in the number of new neurons in the adult hippocampus. *J. Neurosci.* *21*, 1628–1634.
- Tropea, D., Kreiman, G., Lyckman, A., Mukherjee, S., Yu, H., Horng, S., and Sur, M. (2006). Gene expression changes and molecular pathways mediating activity-dependent plasticity in visual cortex. *Nat. Neurosci.* *9*, 660–668.
- Ullrich, A., Gray, A., Tam, A.W., Yang-Feng, T., Tsubokawa, M., Collins, C., Henzel, W., Le Bon, T., Kathuria, S., Chen, E., et al. (1986). Insulin-like growth factor I receptor primary structure: comparison with insulin receptor suggests structural determinants that define functional specificity. *EMBO J.* *5*, 2503–2512.
- Vasilcanu, D., Girnita, A., Girnita, L., Vasilcanu, R., Axelson, M., and Larsson, O. (2004). The cyclolignan PPP induces activation loop-specific inhibition of tyrosine phosphorylation of the insulin-like growth factor-1 receptor. Link to the phosphatidylinositol-3 kinase/Akt apoptotic pathway. *Oncogene* *23*, 7854–7862.
- Verstreken, P., Ly, C.V., Venken, K.J., Koh, T.W., Zhou, Y., and Bellen, H.J. (2005). Synaptic mitochondria are critical for mobilization of reserve pool vesicles at *Drosophila* neuromuscular junctions. *Neuron* *47*, 365–378.
- Vossel, K.A., Beagle, A.J., Rabinovici, G.D., Shu, H., Lee, S.E., Naasan, G., Hegde, M., Cornes, S.B., Henry, M.L., Nelson, A.B., et al. (2013). Seizures and epileptiform activity in the early stages of Alzheimer disease. *JAMA Neurol.* *70*, 1158–1166.
- Wang, G.J., and Thayer, S.A. (2002). NMDA-induced calcium loads recycle across the mitochondrial inner membrane of hippocampal neurons in culture. *J. Neurophysiol.* *87*, 740–749.
- Wang, H., Qin, J., Gong, S., Feng, B., Zhang, Y., and Tao, J. (2014). Insulin-like growth factor-1 receptor-mediated inhibition of A-type K⁺ current induces sensory neuronal hyperexcitability through the phosphatidylinositol 3-kinase and extracellular signal-regulated kinase 1/2 pathways, independently of Akt. *Endocrinology* *155*, 168–179.
- Weiler, S., Krinner, S., Wong, A.B., Moser, T., and Pangrsić, T. (2014). ATP hydrolysis is critically required for function of CaV1.3 channels in cochlear inner hair cells via fueling Ca²⁺ clearance. *J. Neurosci.* *34*, 6843–6848.
- White, R.J., and Reynolds, I.J. (1995). Mitochondria and Na⁺/Ca²⁺ exchange buffer glutamate-induced calcium loads in cultured cortical neurons. *J. Neurosci.* *15*, 1318–1328.
- Wu, L., Bauer, C.S., Zhen, X.G., Xie, C., and Yang, J. (2002). Dual regulation of voltage-gated calcium channels by PtdIns(4,5)P₂. *Nature* *419*, 947–952.
- Xing, C., Yin, Y., Chang, R., Gong, X., He, X., and Xie, Z. (2007). Effects of insulin-like growth factor 1 on synaptic excitability in cultured rat hippocampal neurons. *Exp. Neurol.* *205*, 222–229.
- Yamaguchi, F., Itano, T., Mizobuchi, M., Miyamoto, O., Janjua, N.A., Matsui, H., Tokuda, M., Ohmoto, T., Hosokawa, K., and Hatase, O. (1990). Insulin-like growth factor I (IGF-I) distribution in the tissue and extracellular compartment in different regions of rat brain. *Brain Res.* *533*, 344–347.
- Zhang, B., Tang, X.C., and Zhang, H.Y. (2013). Alternations of central insulin-like growth factor-1 sensitivity in APP/PS1 transgenic mice and neuronal models. *J. Neurosci. Res.* *91*, 717–725.